



Biology and air–sea gas exchange controls on the distribution of carbon isotope ratios ($\delta^{13}\text{C}$) in the ocean

A. Schmittner¹, N. Gruber², A. C. Mix¹, R. M. Key³, A. Tagliabue⁴, and T. K. Westberry⁵

¹College of Oceanic and Atmospheric Sciences, Oregon State University, Corvallis, Oregon, USA

²Institute of Biogeochemistry and Pollutant Dynamics, ETH Zürich, Zürich, Switzerland

³Department of Geosciences, Princeton University, Princeton, New Jersey, USA

⁴School of Environmental Sciences, University of Liverpool, Liverpool, UK

⁵Department of Botany and Plant Pathology, Oregon State University, Corvallis, Oregon, USA

Correspondence to: A. Schmittner (aschmitt@coas.oregonstate.edu)

Received: 3 May 2013 – Published in Biogeosciences Discuss.: 21 May 2013

Revised: 25 July 2013 – Accepted: 25 July 2013 – Published: 4 September 2013

Abstract. Analysis of observations and sensitivity experiments with a new three-dimensional global model of stable carbon isotope cycling elucidate processes that control the distribution of $\delta^{13}\text{C}$ of dissolved inorganic carbon (DIC) in the contemporary and preindustrial ocean. Biological fractionation and the sinking of isotopically light $\delta^{13}\text{C}$ organic matter from the surface into the interior ocean leads to low $\delta^{13}\text{C}_{\text{DIC}}$ values at depths and in high latitude surface waters and high values in the upper ocean at low latitudes with maxima in the subtropics. Air–sea gas exchange has two effects. First, it acts to reduce the spatial gradients created by biology. Second, the associated temperature-dependent fractionation tends to increase (decrease) $\delta^{13}\text{C}_{\text{DIC}}$ values of colder (warmer) water, which generates gradients that oppose those arising from biology. Our model results suggest that both effects are similarly important in influencing surface and interior $\delta^{13}\text{C}_{\text{DIC}}$ distributions. However, since air–sea gas exchange is slow in the modern ocean, the biological effect dominates spatial $\delta^{13}\text{C}_{\text{DIC}}$ gradients both in the interior and at the surface, in contrast to conclusions from some previous studies. Calcium carbonate cycling, pH dependency of fractionation during air–sea gas exchange, and kinetic fractionation have minor effects on $\delta^{13}\text{C}_{\text{DIC}}$. Accumulation of isotopically light carbon from anthropogenic fossil fuel burning has decreased the spatial variability of surface and deep $\delta^{13}\text{C}_{\text{DIC}}$ since the industrial revolution in our model simulations. Analysis of a new synthesis of $\delta^{13}\text{C}_{\text{DIC}}$ measurements from years 1990 to 2005 is used to quantify preformed and remineralized contributions as well as the effects of biol-

ogy and air–sea gas exchange. The model reproduces major features of the observed large-scale distribution of $\delta^{13}\text{C}_{\text{DIC}}$ as well as the individual contributions and effects. Residual misfits are documented and analyzed. Simulated surface and subsurface $\delta^{13}\text{C}_{\text{DIC}}$ are influenced by details of the ecosystem model formulation. For example, inclusion of a simple parameterization of iron limitation of phytoplankton growth rates and temperature-dependent zooplankton grazing rates improves the agreement with $\delta^{13}\text{C}_{\text{DIC}}$ observations and satellite estimates of phytoplankton growth rates and biomass, suggesting that $\delta^{13}\text{C}$ can also be a useful test of ecosystem models.

1 Introduction

The ratio $R = {}^{13}\text{C}/{}^{12}\text{C}$ of the stable carbon isotopes ${}^{13}\text{C}$ and ${}^{12}\text{C}$ in preserved carbonate shells of benthic and planktonic foraminifera is among the most frequently measured quantities from deep-sea sediment core samples. Hence a wealth of data exists on past changes in ${}^{13}\text{C}/{}^{12}\text{C}$ distributions in the ocean (Curry and Oppo, 2005; Sarnthein et al., 2001), typically expressed as the normalized isotopic ratio $\delta^{13}\text{C}$:

$$\delta^{13}\text{C} = (R/R_{\text{std}} - 1) \quad (1)$$

and reported in units of parts per thousand (permil, ‰), where R_{std} is an arbitrary standard ratio, by convention that of the Pee Dee Belemnite, PDB.

Land plants preferentially incorporate ^{12}C relative to ^{13}C into their biomass and typically have $\delta^{13}\text{C}$ of about -28‰ for the C_3 photosynthetic pathway and -14‰ for the C_4 pathway (O'Leary, 1988), substantially depleted in ^{13}C relative to the ambient atmosphere (which is -6 to -7‰). Ocean phytoplankton fractionate similarly resulting in typical $\delta^{13}\text{C}$ of about -21‰ in bulk marine organic matter compared to a mean surface ocean $\delta^{13}\text{C}_{\text{DIC}}$ near 2‰ . In contrast, calcium carbonate (CaCO_3 of corals, benthic shells, or tests of calcareous plankton, i.e. inorganic carbon) has $\delta^{13}\text{C}$ relatively close to that of ambient seawater (Turner, 1982) although reconstructions of past oceanic $\delta^{13}\text{C}_{\text{DIC}}$ from calcareous organisms may be biased by secondary effects such as metabolic rate (Ortiz et al., 1996) and ambient carbonate ion concentration (Spero et al., 1997).

Changes in the global ocean mean of $\delta^{13}\text{C}_{\text{DIC}}$ on geologic timescales ($\geq 10^4$ yr) reflect the balance of erosion and burial of carbonate and organic carbon (Shackleton, 1987; Tschumi et al., 2011; Menviel et al., 2012), while on timescales of up to 10^3 – 10^4 yr they are generally interpreted as changes in the size and composition of the terrestrial (vegetation and soil) active organic carbon pool (Shackleton, 1977). A reduction of terrestrial organic carbon pool, for example, will lead to a release of CO_2 with low $\delta^{13}\text{C}$ into the atmosphere, which will be absorbed by the ocean on the timescale of decades to centuries. Ultimately the isotopic composition of the atmosphere is controlled by the near-surface seawater isotopic composition, because the ocean contains $> 90\%$ of the actively exchangeable carbon in the ocean-land-atmosphere system (Houghton, 2007). An improved quantification of the processes that control the distribution of carbon isotopes within the ocean as well as ocean-sediment interactions will therefore enable better understanding of long-term sources and sinks of CO_2 (Schmitt et al., 2012).

In paleoceanographic records, the vertical gradients in $\delta^{13}\text{C}_{\text{DIC}}$ between the warm surface ocean (planktonic foraminifera) and average deep ocean (benthic foraminifera) are generally assumed to reflect the integrated efficiency of the ocean's biological soft-tissue pump (Shackleton et al., 1992; Broecker, 1982; Berger and Vincent, 1986). Variations in spatial gradients of deep-ocean $\delta^{13}\text{C}_{\text{DIC}}$ are frequently attributed to circulation changes (e.g., Curry and Oppo, 2005) although it has long been known that changes in the preformed properties of paleo-deep water masses are possible (Mix and Fairbanks, 1985; Broecker and Maier-Reimer, 1992; Lynch-Stieglitz and Fairbanks, 1994). Deep-water $\delta^{13}\text{C}_{\text{DIC}}$ in the contemporary ocean is roughly anti-correlated with nutrient concentrations such as phosphate or nitrate (Broecker and Maier-Reimer, 1992), and with apparent oxygen utilization (AOU; Kroopnick, 1985). These properties, in turn, reflect differences in preformed properties associated with water mass formation, the accumulation of remineralized organic matter during the time elapsed since isolation from the sea surface, and subsurface mixing between different water masses (Broecker and Maier-Reimer,

1992). Nutrient concentrations in North Atlantic Deep Water (NADW), for example, are low (with high $\delta^{13}\text{C}_{\text{DIC}}$) because NADW has recently been sinking from the surface (where nutrients are depleted by phytoplankton), whereas they are high (and $\delta^{13}\text{C}_{\text{DIC}}$ is low) in Pacific Deep Water, which is old and has accumulated a large amount of remineralized organic matter. $\delta^{13}\text{C}_{\text{DIC}}$ and nutrient cycles are linked through phytoplankton growth at the sea surface, which leads to the uptake of inorganic nutrients and isotopically light carbon. This leaves the remaining surface seawater enriched in $\delta^{13}\text{C}_{\text{DIC}}$ and depleted in nutrients. Upon remineralization at depths, carbon of low $\delta^{13}\text{C}$ is released proportional to the release of nutrients, decreasing $\delta^{13}\text{C}_{\text{DIC}}$ and enriching nutrient concentrations there.

Some of the large changes in $\delta^{13}\text{C}$ observed for the past, such as during the Last Glacial Maximum (LGM) Atlantic Ocean (Curry and Oppo, 2005; Sarnthein et al., 2001), strongly suggest changed circulation patterns. A recent inverse modeling study showed that, under certain assumptions, the LGM $\delta^{13}\text{C}$ distribution in the deep Atlantic is inconsistent with the modern flow field (Marchal and Curry, 2008). However, $\delta^{13}\text{C}$ is in no simple way related to the circulation rate (Legrand and Wunsch, 1995); effects of air-sea gas exchange (Broecker and Maier-Reimer, 1992), variations in the isotopic discrimination during photosynthesis (Goericke and Fry, 1994), and minor buffering by dissolution of calcium carbonate complicate the interpretation of $\delta^{13}\text{C}$ as a direct nutrient or ventilation proxy. Interpretation of paleodata on oceanic $\delta^{13}\text{C}$ is sufficiently complex that a model is needed to deconvolve these various contributions to the record in physically consistent ways.

Here we include ^{13}C cycling directly as prognostic variables in a model of the ocean-atmosphere system, including quantitative descriptions of the fractionation processes. A combination of data and models can then be used to infer the interplay of ocean circulation and isotopic biogeochemistry and to quantify past changes in global ocean carbon cycling. As a first step, such a model needs to be carefully compared to the large amount of existing data from the contemporary ocean, which is an important purpose of this paper. Previous modeling studies have compared different aspects of the simulated ^{13}C cycle with modern observations (Tagliabue and Bopp, 2008; Hofmann et al., 2000; Marchal et al., 1998) but a comprehensive comparison with inorganic and organic carbon isotope measurements has not yet been undertaken. A large number of new measurements that have dramatically increased the data coverage for the modern ocean are now available. Here we present a global compilation of these new measurements of $\delta^{13}\text{C}_{\text{DIC}}$, analyzed from 1990 to 2005.

We consider three controls on $\delta^{13}\text{C}$ distribution in the modern (preindustrial) ocean: (1) biological effects, (2) air-sea gas exchange and (3) the degree of isotopic disequilibrium between the surface ocean and the atmosphere, which is longer (~ 10 yr) than the air-sea equilibration

time-scale for CO_2 (~ 1 yr) (Broecker and Peng, 1982). Previous work has examined some of the important aspects of these processes. Broecker and Maier-Reimer (1992) note that the temperature-dependent equilibrium fractionation during air–sea gas exchange, which leads to lower $\delta^{13}\text{C}_{\text{DIC}}$ values at higher temperatures, opposes the effect of biological fractionation. However, the temperature effect is moderated by slow air–sea gas exchange. They conclude that for the modern surface ocean the temperature effect largely compensates the biological effect, whereas for the deep ocean the biological effect dominates. These conclusions were confirmed by Lynch-Stieglitz et al. (1995), who analyzed observations and simulations with a model without biology, and Gruber et al. (1999) who analyzed surface observations. Murnane and Sarmiento (2000; MS00 in the following) used a series of model simulations with and without biology and with regular and infinitely fast gas exchange. They concluded that air–sea gas exchange is more important than biology for surface $\delta^{13}\text{C}_{\text{DIC}}$. No previous study has, to our knowledge, quantified the effects of non fractionating air–sea exchange acting on biologically created gradients or the effect of CaCO_3 cycling. Here we present model experiments designed to quantify these effects. A new analysis of observations and model results re-examines the relative importance of biology and gas exchange effects on the $\delta^{13}\text{C}_{\text{DIC}}$ distribution in the preindustrial and contemporary ocean, given modern physical circulation patterns.

2 Model description

The physical and marine ecosystem models used here are described and validated in detail elsewhere (Schmittner et al., 2008, 2009a). The three-dimensional ocean general circulation model component of the UVic Earth System Model (Weaver et al., 2001), here we use version 2.8, solves the primitive equations at a relatively coarse spatial resolution ($1.8 \times 3.6^\circ$, 19 vertical levels) and is coupled to a one-layer energy-moisture balance atmospheric model and a dynamic thermodynamic sea ice model. In deviating from Schmittner et al. (2009a), here we do not use enhanced dia-pycnal mixing in the Southern Ocean, which led to too high $\delta^{13}\text{C}_{\text{DIC}}$ in the deep ocean. Rather we use a slightly higher background diapycnal diffusivity of $K_{\text{bg}} = 0.2 \times 10^{-4} \text{ m}^2 \text{ s}^{-1}$ (Schmittner et al., 2009 used $K_{\text{bg}} = 0.15 \times 10^{-4} \text{ m}^2 \text{ s}^{-1}$). The biogeochemical model includes interactive nitrogen, phosphorous, oxygen and carbon cycles, but it does not include either silicate or iron (although we include a sensitivity test that addresses potential issues of iron fertilization). Ecosystem model parameters are as in Schmittner et al. (2008) amended by Schmittner et al. (2009b) except for $R_{\text{CaCO}_3/\text{POC}} = 0.025$, $a_{\text{P}_0} = 0.5$, $a_{\text{P}_D} = 0.08$, $g = 0.6$, $\epsilon = 2$, $k_c = 0.047$, $w_D = 7$, $D_{\text{CaCO}_3} = 4500$, and $\mu_{\text{P}_0} = 0.01$ (model *FeL*, for units and descriptions see original papers). Model *std* uses the same parameters as *FeL* except for $g = 1.575$, and $\epsilon = 15$.

In addition to equations for total carbon ($\text{C} = {}^{12}\text{C} + {}^{13}\text{C} \cong {}^{12}\text{C}$), which we assume to approximate ${}^{12}\text{C}$ since ${}^{13}\text{C}$ comprises only about 1.1 % of total C and ${}^{14}\text{C}$ is present only in trace quantities, the isotope ${}^{13}\text{C}$ has been implemented in all five prognostic carbon variables of the ocean component of the model, that is, in two phytoplankton classes (nitrogen fixers and a general phytoplankton class), zooplankton, detritus and DIC. Fractionation is considered during air–sea gas exchange and during photosynthetic carbon uptake by phytoplankton. In the model $R_{\text{std}} = 1$ (Eq. 1) is used in order to minimize numerical errors. Particulate organic matter/carbon (POM/C, detritus) sinks in the model with a depth dependent sinking speed and is remineralized with a linear (first order) constant rate, which leads to an approximately exponential remineralization with an e-folding depth of a few hundred meters. Inorganic carbon (CaCO_3), on the other hand, is not simulated as a prognostic variable. CaCO_3 production is calculated as a constant fraction of production of POC and instantaneously dissolved in the deep ocean with an e-folding depth of 4.5 km.

2.1 Air–sea gas exchange

The flux of total $\text{CO}_2 = {}^{12}\text{CO}_2 + {}^{13}\text{CO}_2$ in $\text{mol m}^{-2} \text{ s}^{-1}$ across the air–sea interface follows the Ocean Carbon Model Intercomparison Project guidelines (Orr et al., 2000)

$$F_{\text{C}} = -k(C_{\text{surf}} - C_{\text{sat}}), \quad (2)$$

where C_{surf} is the surface aqueous CO_2 concentration, C_{sat} is the saturation concentration corresponding to atmospheric $p\text{CO}_2$, both in mol m^{-3} , and the piston velocity in m s^{-1}

$$k = k_0(1 - a_{\text{ice}})u^2(S_c/660)^{-0.5} \quad (3)$$

depends on fractional sea ice cover within a grid box a_{ice} , wind speed u in m s^{-1} , and the sea–surface temperature (SST in $^\circ\text{C}$) dependent Schmidt number for CO_2 , $S_c = 2073.1 - 125.62 \cdot \text{SST} + 3.6276 \cdot \text{SST}^2 - 0.043219 \cdot \text{SST}^3$. Here we use tunable parameter $k_0 = 0.253$ in the default model, which is close to recently updated estimates (0.27) based on radiocarbon (Sweeney et al., 2007; Graven et al., 2012) and 25 % smaller than the value of 0.337 used in previous studies with this model (Schmittner et al., 2008). A 25 % reduced air–sea gas exchange leads to about a 0.1 ‰ lower global mean $\delta^{13}\text{C}_{\text{DIC}}$ and 14 ‰ reduction in global mean $\Delta^{14}\text{C}$ in our model. Note that the $\Delta^{14}\text{C}$ simulation is consistent with observations and similar, perhaps even slightly improved, compared to that of Schmittner et al. (2008), who used the previous UVic model version 2.7, for which various parameters (e.g. in the atmospheric component) were different.

The air–sea flux of ${}^{13}\text{CO}_2$ ($F_{13\text{C}}$) is calculated according to Zhang et al. (1995):

$$F_{13\text{C}} = -k\alpha_k\alpha_{\text{aq}\leftarrow\text{g}} \left(\frac{R_{\text{DIC}}}{\alpha_{\text{DIC}\leftarrow\text{g}}} C_{\text{surf}} - R_{\text{A}} C_{\text{sat}} \right). \quad (4)$$

The first term in the brackets on the right-hand side represents outgassing of oceanic ^{13}C to the atmosphere ($\alpha_{\text{aq}\leftarrow\text{g}}/\alpha_{\text{DIC}\leftarrow\text{g}} = \alpha_{\text{aq}\leftarrow\text{DIC}}$) and is a loss of $^{13}\text{C}_{\text{DIC}}$ from the surface model grid box, and the second term represents invasion of atmospheric ^{13}C into the ocean and is a source of $^{13}\text{C}_{\text{DIC}}$ for the surface model grid box. $\alpha_k = 0.99915$ is a constant kinetic fractionation factor. Here we neglect the minor temperature dependency of the isotopic fractionation factor from gaseous to aqueous CO_2 ($5 \times 10^{-6} \text{ }^\circ\text{C}$) found by Zhang et al. (1995) and approximate it as a constant $\alpha_{\text{aq}\leftarrow\text{g}} = 0.998764$ corresponding to a mean temperature of $15 \text{ }^\circ\text{C}$.

$$\alpha_{\text{DIC}\leftarrow\text{g}} = 1.01051 - 1.05 \times 10^{-4} T \quad (5)$$

is the temperature (in $^\circ\text{C}$)-dependent equilibrium fractionation factor from gaseous CO_2 to DIC. $R_{\text{DIC}} = {}^{13}\text{C}_{\text{DIC}}/({}^{12}\text{C}_{\text{DIC}} + {}^{13}\text{C}_{\text{DIC}})$ is the heavy to total isotope ratio of DIC, $R_{\text{A}} = {}^{13}\text{C}_{\text{CO}_2}/({}^{12}\text{C}_{\text{CO}_2} + {}^{13}\text{C}_{\text{CO}_2})$ is the heavy to total isotope ratio of atmospheric CO_2 .

Here we use Zhang et al.'s (1995) direct measurements of $\alpha_{\text{DIC}\leftarrow\text{g}}$ in sea water (their Fig. 6), rather than their fractionation factors for the individual carbonate species measured in freshwater sodium bicarbonate solutions. Zhang et al. (1995) show that their individual fractionation factors cannot be used to calculate $\alpha_{\text{DIC}\leftarrow\text{g}}$, which they attribute to the presence of other carbonate complexes in sea water. They also found a secondary dependency of $\alpha_{\text{DIC}\leftarrow\text{g}}$ on pH, which they expressed as a function of the carbonate ion fraction f_{CO_3} . In the modern surface ocean f_{CO_3} varies from about 5 % at high latitudes to about 20 % at low latitudes. This would cause $\alpha_{\text{DIC}\leftarrow\text{g}}$ to be about 0.05 ‰ higher in the tropics than at the poles. This is much smaller than the 3 ‰ effect of temperature alone. A sensitivity experiment including the pH effect showed a small (0.05 ‰) increase in simulated $\delta^{13}\text{C}_{\text{DIC}}$ in tropical surface waters after 1000 years of simulation. For all experiments presented in the remainder of this paper this effect has been neglected. For paleo-applications in which dramatic changes in f_{CO_3} can be expected it will be easy to include this effect.

2.2 Photosynthesis

Isotopic fractionation during photosynthesis is

$$\alpha_{\text{POC}\leftarrow\text{DIC}} = \alpha_{\text{aq}\leftarrow\text{DIC}} \alpha_{\text{POC}\leftarrow\text{aq}} = \frac{\alpha_{\text{aq}\leftarrow\text{g}}}{\alpha_{\text{DIC}\leftarrow\text{g}}} \alpha_{\text{POC}\leftarrow\text{aq}}, \quad (6)$$

where the equilibrium fractionation factor from aqueous CO_2 to particulate organic carbon (POC) depends on the partial pressure of CO_2 in surface water; according to Popp et al. (1989):

$$\alpha_{\text{POC}\leftarrow\text{aq}} = -0.017 \log(C_{\text{surf}}) + 1.0034. \quad (7)$$

Initial results with the more process-based (but more complex formulation, based on diffusive CO_2 uptake by phytoplankton from Rau et al. (1996)), which considers phytoplankton growth rates and other variables, did not yield better

results. This may be due to difficulties of the current model version in simulating the correct phytoplankton growth rates, as a comparison with satellite estimates (Westberry et al., 2008) suggests (Fig. 1). A controversial issue remains as to what degree phytoplankton actively acquire CO_2 or bicarbonate, which could affect carbon isotope fractionation differently from a passive, diffusive uptake model (Keller and Morel, 1999).

The effects of biological fractionation of stable carbon isotopes in organic matter are reported as the isotopic enrichment factor

$$\varepsilon = \alpha - 1. \quad (8)$$

Large variations of isotopic enrichment factors have been reported for different phytoplankton species. Diazotrophs (nitrogen fixing microorganisms) in particular appear to show low fractionation factors (Carpenter et al., 1997). Test simulations with a fractionation factor of 12 ‰ for diazotrophs showed small effects (< 0.1 ‰) on the global $\delta^{13}\text{C}_{\text{DIC}}$ distributions, primarily because of the small direct contribution of diazotrophic organisms to global biomass and primary production. Hence this effect was not included in the default model version.

Fractionation during production of calcium carbonate is small (Turner, 1982) and not considered here (i.e., $\delta^{13}\text{C}_{\text{CaCO}_3}$ is assumed equal to the $\delta^{13}\text{C}_{\text{DIC}}$ of the surface water mass where it formed). However, the CaCO_3 pump impacts $\delta^{13}\text{C}_{\text{DIC}}$ by the transport of carbon from the surface to the deep ocean, because calcite dissolves deeper than organic matter, although, as we evaluate below, this effect is small.

3 Sensitivity experiments

We have performed twelve sensitivity experiments (Table 1) designed to quantify the effects of individual processes on the simulated $\delta^{13}\text{C}_{\text{DIC}}$ distribution (#1–#11) and to illustrate the effect of structural changes in details of the ecosystem model formulation (#12; *FeL*). In addition to the standard full model (*std*, which corresponds to the “OBM” of MS00) simulations without biological fractionation (*no-bio*, $\alpha_{\text{POC}\leftarrow\text{DIC}} = 1$; which corresponds to the “Solubility Model” of MS00), with only kinetic fractionation (*ki-only*), without gas exchange (*no-gasx*), and without fractionation during air–sea gas exchange (*const-gasx*) are used to quantify the effects of those processes.

Models *fast-gasx-only*, *bio-fast*, and *fast-gasx* explore the role of much faster gas exchange (twenty times the standard rate for both ^{13}C and total C) alone, with biological fractionation, and with both biological and kinetic fractionation, respectively. (Our experiments *fast-gasx-only* and *fast-gasx* are analogous to the “Potential Solubility Model” and “Potential OBM” of MS00, respectively.) The fast gas exchange experiments approach the limit of infinitely fast gas exchange, which was determined analytically

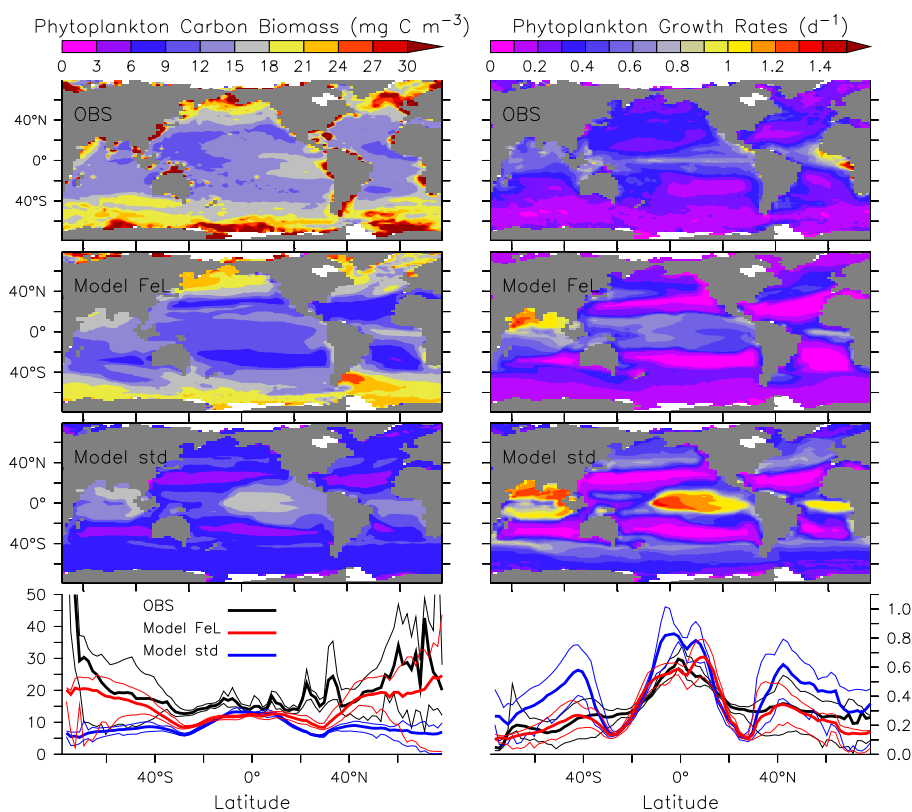


Fig. 1. Annual mean surface (0–50 m) phytoplankton carbon biomass (left) and growth rates (right) from satellite estimates (top, Westberry et al., 2008) and two models. Model *FeL* uses temperature-dependent zooplankton growth rates ($Q_{10} = 1.9$, $g(T = 0^\circ\text{C}) = 0.6 \text{ d}^{-1}$) and a simple parameterization of iron limitation of phytoplankton growth rates similar to that used by Somes et al. (2010), which modulates maximum phytoplankton growth rates by aeolian iron flux (Mahowald et al., 2005). Whereas Somes et al. (2010) used iron limitation only for diazotrophs, here we also apply it to other phytoplankton. Whereas non-diazotroph phytoplankton's growth rates are linearly reduced by up to 60 % for iron fluxes less than $1 \text{ g m}^{-2} \text{ yr}^{-1}$, diazotroph's growth rates are reduced by up to 80 %, accounting for their higher iron requirements. Model *std* uses no temperature dependence of zooplankton growth rates and no parameterization of iron limitation. Bottom panels show zonally averaged values (thick lines), including the annual minimum and maximum (thin lines) to indicate the amplitude of the seasonal cycle. Annual averages have been calculated using monthly model output only at those grid points where observations are available for that month. At high latitudes the satellite data are biased toward summer. Maximum zooplankton growth rates of model *FeL* are consistent with results from incubation experiments (Hansen and Jensen, 2000).

as $\delta^{13}\text{C}_{\text{DIC,inf-gasx-only}} = 3.9\text{‰} - 0.1\text{‰} (\text{°C})^{-1} \cdot \text{SST}$, where $0.1\text{‰} (\text{°C})^{-1}$ is the slope of the temperature dependence of Eq. (5) and the constant 3.9‰ adjusts the global mean surface $\delta^{13}\text{C}_{\text{DIC}}$ to be equal to that of model *fast-gasx-only*. Model *no-gasx* has gas exchange of carbon between ocean and atmosphere set to zero. Experiments 9–11 assume different values for a spatially constant biological fractionation factor.

Experiment 12, *FeL*, uses a simple parameterization of iron limitation of phytoplankton and temperature-dependent grazing rates of zooplankton on phytoplankton similar to the independent approach by Keller et al. (2012), who show that these changes improve the seasonality of phytoplankton blooms. Here we use a map of dust fluxes (Mahowald et al., 2005) to scale maximum phytoplankton growth rates and do not limit the increase of zooplankton grazing with tempera-

ture above 20°C whereas Keller et al. (2012) used dissolved iron concentrations in sea water simulated by a model with an interactive iron cycle. We acknowledge that dust may not be the only important source of available iron as a micronutrient (Elrod et al., 2004; Boyd and Ellwood, 2010). Nevertheless, in Fig. 1 we show that this relatively simple addition to the model improves the simulation of phytoplankton growth rates and carbon biomass as judged from a comparison with satellite estimates of these quantities (Westberry et al., 2008).

All model simulations were initiated from a 6800 yr-long spin up simulation of model *std*, which itself was initiated with $\delta^{13}\text{C}_{\text{DIC}} = 0$ everywhere, and subsequently integrated for 4000 yr or more (7000 and 8000 yr for *fast-gasx-only* and *ki-only*) with a prescribed preindustrial value for atmospheric CO_2 of $\delta^{13}\text{C}_{\text{CO}_2,\text{atm}} = -6.5\text{‰}$ (Francey et al., 1999)

Table 1. Sensitivity experiments. Note that 4a is not a numerical experiment but the results were calculated using simulated temperature as described in the text.

Experiment	Biol. fract. $\alpha_{\text{POC} \leftarrow \text{DIC}}$ Eq. (6)	Equil. fract. $\alpha_{\text{aq} \leftarrow g}, \alpha_{\text{DIC} \leftarrow g}$ Eq. (4)	Kin. fract. α_k	Gas exchange k_0
1. <i>std</i>	var-std	var-std	std (0.99915)	std (0.253)
2. <i>no-bio</i>	1	var-std	std	std
3. <i>ki-only</i>	1	1	std	std
4. <i>fast-gasx-only</i>	1	var-std	1	fast ($20 \times \text{std} = 5.06$)
(4a. <i>inf-gasx-only</i>)	1	var-std	1	infinite)
5. <i>no-gasx</i>	var-std	NA	NA	0
6. <i>const-gasx</i>	var-std	1	1	std
7. <i>bio-fast</i>	var-std	var-std	1	fast
8. <i>fast-gasx</i>	var-std	var-std	std	fast
9. <i>low-bio</i>	0.980	var-std	std	std
10. <i>med-bio</i>	0.975	var-std	std	std
11. <i>high-bio</i>	0.970	var-std	std	std
12. <i>FeL</i>	as std but with iron limitation of phytoplankton growth (see text)			

until equilibrium was approximated. The last 100 yr of these preindustrial control simulations are presented in Sect. 5.1.

The anthropogenic release of low $\delta^{13}\text{C}$ fossil carbon into the atmosphere since the industrial revolution has led to a transient decrease of atmospheric $\delta^{13}\text{C}_{\text{CO}_2}$ by about 1.5‰ between preindustrial background and the year 2000 (“ $\delta^{13}\text{C}$ Suess Effect”, Fig. 2); the effect on the surface ocean has been smaller, and spatially variable due to mixing with subsurface water masses, but still significant. For our simulations of the historical anthropogenic period we use the observed atmospheric CO_2 and $\delta^{13}\text{C}_{\text{CO}_2, \text{atm}}$ from year 1800 to year 2000 derived from measurements of atmospheric air samples, as well as air samples extracted from Antarctic firn and ice (Allison and Francey, 1999; Francey et al., 1999), as a surface boundary condition (Fig. 2) in addition to climate forcing estimates (Crowley, 2000).

4 Analysis of preformed and remineralized $\delta^{13}\text{C}$, effects of biology and air–sea gas exchange

Following previous studies (Kroopnick, 1985; Gruber et al., 1999; Broecker, 1974) it is useful to separate total DIC

$$\text{DIC} \cong {}^{12}\text{C}_{\text{DIC}} = {}^{12}\text{C}_{\text{pre}} + {}^{12}\text{C}_{\text{org}} + {}^{12}\text{C}_{\text{CaCO}_3} \quad (9)$$

and ^{13}C

$${}^{13}\text{C}_{\text{DIC}} = {}^{13}\text{C}_{\text{pre}} + {}^{13}\text{C}_{\text{org}} + {}^{13}\text{C}_{\text{CaCO}_3} \quad (10)$$

into preformed components (${}^{12}\text{C}_{\text{pre}}, {}^{13}\text{C}_{\text{pre}}$) that arise from advection of surface waters with specific ${}^{12}\text{C}_{\text{DIC}}$ and ${}^{13}\text{C}_{\text{DIC}}$ values into the interior ocean and remineralized components ${}^{12}\text{C}_{\text{rem}} = {}^{12}\text{C}_{\text{org}} + {}^{12}\text{C}_{\text{CaCO}_3}$ and ${}^{13}\text{C}_{\text{rem}} = {}^{13}\text{C}_{\text{org}} + {}^{13}\text{C}_{\text{CaCO}_3}$ that arise from the addition of isotopically light carbon from remineralization of organic matter ($\delta^{13}\text{C}_{\text{org}} \cong -21\text{‰}$) and

isotopically heavy carbon from the dissolution of calcium carbonate ($\delta^{13}\text{C}_{\text{CaCO}_3} \cong 2\text{‰}$) during the transit time of that water mass. The remineralized organic portions can be approximated as

$${}^{12}\text{C}_{\text{org}} = r_{\text{C}:\text{O}} \text{AOU} \quad (11)$$

$${}^{13}\text{C}_{\text{org}} = R_{\text{org}} {}^{12}\text{C}_{\text{org}}, \quad (12)$$

where $\text{AOU} = \text{O}_2^{\text{sat}} - \text{O}_2$, O_2^{sat} is the temperature and salinity-dependent saturation concentration for dissolved oxygen, $r_{\text{C}:\text{O}} = 0.66$ is the stoichiometric ratio of carbon to oxygen for the production/remineralization of organic matter (Anderson and Sarmiento, 1994), and R_{org} is the ratio of isotopically heavy over total organic carbon. The inorganic portions are

$${}^{12}\text{C}_{\text{CaCO}_3} = p\text{ALK}_{\text{dis}}/2 \quad (13)$$

$${}^{13}\text{C}_{\text{CaCO}_3} = R_{\text{CaCO}_3} {}^{12}\text{C}_{\text{CaCO}_3}, \quad (14)$$

where $p\text{ALK}_{\text{dis}} = p\text{ALK} - p\text{ALK}_{\text{pre}}$ is the dissolved portion of the potential alkalinity $p\text{ALK} = (\text{ALK} + \text{NO}_3) \cdot 35/S$, i.e. the difference from its preformed value $p\text{ALK}_{\text{pre}}$, and R_{CaCO_3} is the ratio of isotopically heavy over total CaCO_3 .

Equations (9) and (10) can be combined to yield

$$\delta^{13}\text{C}_{\text{DIC}} = \frac{1}{{}^{12}\text{C}_{\text{DIC}}} \left(\delta^{13}\text{C}_{\text{pre}} {}^{12}\text{C}_{\text{pre}} + \delta^{13}\text{C}_{\text{org}} {}^{12}\text{C}_{\text{org}} + \delta^{13}\text{C}_{\text{CaCO}_3} {}^{12}\text{C}_{\text{CaCO}_3} \right), \quad (15)$$

which expresses the total $\delta^{13}\text{C}_{\text{DIC}}$ of a water parcel by the mass-fraction (e.g. ${}^{12}\text{C}_{\text{pre}}/{}^{12}\text{C}_{\text{DIC}}$) weighted contributions from preformed and remineralized components (Kroopnick, 1985). All terms in Eq. (15) can be estimated except $\delta^{13}\text{C}_{\text{pre}}$,

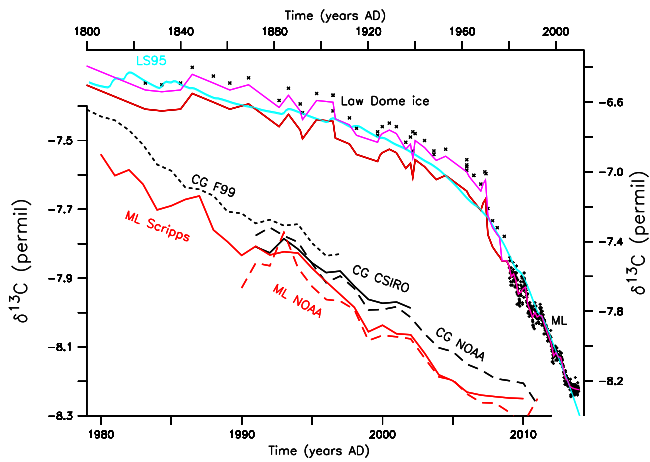


Fig. 2. Main panel (top and right axes): evolution of $\delta^{13}\text{C}_{\text{CO}_2, \text{atm}}$ from 1800 to 2010 used for the model forcing (red solid line) and original data from the Law Dome ice core (x-symbols) and air samples from Mauna Loa, Hawaii measured at Scripps Institution of Oceanography (Keeling et al., 2001) (plus symbols). 0.15 ‰ have been subtracted from the ice core measurements. This correction is applied in order to match with the Mauna Loa data and justified in part due to the observed gradient (~ 0.7 ‰) between the high latitude Southern Hemisphere data and those from the tropics shown in the inset panel and partly due to biases in the ice core measurements as determined by comparison to the firm and air sample measurements. The purple and light blue lines show alternative forcing functions derived by adjusting the ice core data by $\Delta\delta^{13}\text{C} = -0.04$ ‰ and using the relation of $\delta^{13}\text{C} = -1.4$ ‰ $- P_A \cdot 0.0182$ ‰ ppm^{-1} with atmospheric CO_2 (P_A) proposed by (Lynch-Stieglitz et al., 1995).

Inset panel (bottom and left axis): $\delta^{13}\text{C}$ of atmospheric CO_2 in air from Mauna Loa measured at National Oceanographic and Atmospheric Administration (NOAA) (White and Vaughn, 2011) (red dashed line), and air samples at Cape Grim, Tasmania from Francey et al. (1999) (black dotted line) and from Allison and Francey (1999) (black solid line) and from (White and Vaughn, 2011). All lines show annual mean data calculated by averaging the raw data on a regular yearly grid.

which we calculate as a residual

$$\delta^{13}\text{C}_{\text{pre}} = \frac{1}{^{12}\text{C}_{\text{pre}}} \left(\delta^{13}\text{C}_{\text{DIC}} \text{ } ^{12}\text{C}_{\text{DIC}} - \delta^{13}\text{C}_{\text{Org}} \text{ } ^{12}\text{C}_{\text{Org}} - \delta^{13}\text{C}_{\text{CaCO}_3} \text{ } ^{12}\text{C}_{\text{CaCO}_3} \right). \quad (16)$$

Similarly $^{12}\text{C}_{\text{pre}}$ is calculated as the residual from Eq. (9). Note that we use $\delta^{13}\text{C}_{\text{Org}} = -21$ ‰ and $\delta^{13}\text{C}_{\text{CaCO}_3} = 2$ ‰ for all experiments except for *const-gasx*, for which we use $\delta^{13}\text{C}_{\text{Org, const-gasx}} = \text{mean}(\delta^{13}\text{C}_{\text{detr}} (z = 0 : 100 \text{ m})) = -29.6$ ‰ and $\delta^{13}\text{C}_{\text{CaCO}_3, \text{const-gasx}} = \text{mean}(\delta^{13}\text{C}_{\text{DIC, const-gasx}} (z = 0 : 100 \text{ m})) = -6.5$ ‰, and for *no-bio* and *fast-gasx-only* $\delta^{13}\text{C}_{\text{Org, no-bio}} = \delta^{13}\text{C}_{\text{Org, fast-gasx-only}} = \text{mean}(\delta^{13}\text{C}_{\text{DIC}} (z = 0 : 100 \text{ m})) = 2$ ‰.

Gruber et al. (1999) proposed the following separation into biological and air–sea gas exchange components

$$\text{DIC} = \text{C}^* + \text{C}_{\text{bio}} \quad (17)$$

$$^{13}\text{C}_{\text{DIC}} = ^{13}\text{C}^* + ^{13}\text{C}_{\text{bio}}, \quad (18)$$

where $\text{C}_{\text{bio}} = \text{C}_{\text{soft}} + \text{C}_{\text{hard}}$, $\text{C}_{\text{soft}} = r_{\text{C:P}} \Delta \text{PO}_4$ with $r_{\text{C:P}} = 112$, $\text{C}_{\text{hard}} = \Delta p\text{ALK}/2$, $^{13}\text{C}_{\text{soft}} = R_{\text{org}} \text{C}_{\text{soft}}$, and $^{13}\text{C}_{\text{hard}} = R_{\text{CaCO}_3} \text{C}_{\text{hard}}$, $\Delta \text{PO}_4 = \text{PO}_4 - \text{PO}_4^0$, and $\Delta p\text{ALK} = p\text{ALK} - p\text{ALK}^0$. PO_4^0 and $p\text{ALK}^0$ are constant reference values. Here we use the global mean surface values. Analogous to Eq. (15) we get

$$\delta^{13}\text{C}_{\text{DIC}} = \frac{1}{^{12}\text{C}_{\text{DIC}}} \left(\delta^{13}\text{C}^* \text{C}^* + \delta^{13}\text{C}_{\text{org}} \text{C}_{\text{soft}} + \delta^{13}\text{C}_{\text{CaCO}_3} \text{C}_{\text{hard}} \right). \quad (19)$$

Analogous to the calculation of $\delta^{13}\text{C}_{\text{pre}}$ (Eq. 16) $\delta^{13}\text{C}^*$ can be evaluated as the residual. Note that the delta values themselves are not additive. Nevertheless, Gruber et al. (1999) define the effect of biology as the difference

$$\Delta\delta^{13}\text{C}_{\text{bio}} \equiv \delta^{13}\text{C}_{\text{DIC}} - \delta^{13}\text{C}^*. \quad (20)$$

We will assess this approximation of biological effects by comparing to our simulation without gas exchange (*no-gasx*), which is only influenced by biology ($\delta^{13}\text{C}_{\text{bio}} = \delta^{13}\text{C}_{\text{DIC, no-gasx}}$).

$\delta^{13}\text{C}_{\text{pre}}$ and $^{12}\text{C}_{\text{pre}}$ are related to $\delta^{13}\text{C}^*$ and C^* by the following equations:

$$^{12}\text{C}_{\text{pre}} = \text{C}^* + r_{\text{C:P}} \Delta \text{PO}_{4, \text{pre}} + \Delta p\text{ALK}_{\text{pre}}/2 \quad (21)$$

$$\delta^{13}\text{C}_{\text{pre}} = \frac{1}{^{12}\text{C}_{\text{pre}}} \left(\delta^{13}\text{C}^* \text{C}^* + \delta^{13}\text{C}_{\text{Org}} r_{\text{C:P}} \Delta \text{PO}_{4, \text{pre}} + \delta^{13}\text{C}_{\text{CaCO}_3} \Delta p\text{ALK}_{\text{pre}}/2 \right), \quad (22)$$

where $\Delta \text{PO}_{4, \text{pre}} = \text{PO}_{4, \text{pre}} - \text{PO}_{4, \text{pre}}^0$ is the difference of the preformed phosphate concentration $\text{PO}_{4, \text{pre}} = \text{PO}_4 - r_{\text{P:O}} \text{AOU}$ from some reference value $\text{PO}_{4, \text{pre}}^0$ and $r_{\text{P:O}} = r_{\text{C:O}}/r_{\text{C:P}}$. Here we use the global mean surface phosphate as $\text{PO}_{4, \text{pre}}^0$. Equations (21) and (22) illustrate that the definitions of $\delta^{13}\text{C}^*$ and C^* remove not only the remineralized biological carbon but also the components associated with preformed phosphate and alkalinity.

The effect of air–sea fluxes on surface $\delta^{13}\text{C}$ tendencies can be approximated by the difference between the fluxes of ^{13}C (divided by the standard isotopic ratio) and total C:

$$\Delta F_{^{13}\text{C}} = F_{^{13}\text{C}}/R_{\text{std}} - F_{\text{C}}, \quad (23)$$

such that positive values of the difference in isotope flux $\Delta F_{^{13}\text{C}}$ would tend to increase surface ocean $\delta^{13}\text{C}$. Assuming

no fractionation during air–sea gas exchange (i.e. all fractionation factors in Eq. (4) are equal to one) and using Eqs. (2) and (4) $\Delta F_{13\text{C}}$ becomes

$$\Delta F_{13\text{C, const-gasx}} = -k(\delta^{13}\text{C}_{\text{DIC, surf}} - \delta^{13}\text{C}_{\text{A, Csat}}). \quad (24)$$

Equation (24) illustrates that air–sea fluxes will affect surface $\delta^{13}\text{C}$ even in the case of no fractionation during air–sea gas exchange if $\delta^{13}\text{C}_{\text{DIC, surf}} \neq \delta^{13}\text{C}_{\text{A, Csat}}$. Thus, differences between the surface ocean and atmosphere in either, $\delta^{13}\text{C}$, $p\text{CO}_2$, or both, can cause a difference isotope flux. Since biology affects both, it will also influence $\Delta F_{13\text{C}}$.

We will see below that kinetic fractionation has a negligible influence on the $\delta^{13}\text{C}$ distribution in the ocean. Similarly the sinking of calcium carbonate has only a minor impact. Therefore these two processes will be neglected in the remainder of the analysis presented in this subsection. In order to separate the effect of biology on air–sea fluxes from those generated by the temperature-dependent fractionation we write

$$^{13}\text{C}^* = ^{13}\text{C}_{\text{bio}}^* + ^{13}\text{C}_T^*, \quad (25)$$

where the temperature-dependent part can be further separated into an equilibrium and a disequilibrium part:

$$^{13}\text{C}_T^* = ^{13}\text{C}_{T, \text{eq}}^* + ^{13}\text{C}_{T, \text{dis}}^*. \quad (26)$$

The equilibrium part $^{13}\text{C}_{T, \text{eq}}^*$ will be the same for all experiments and only depend on temperature, whereas the disequilibrium part $^{13}\text{C}_{T, \text{dis}}^*$ will depend on the air–sea gas exchange rate such that it is large for slow and small for fast rates. For infinitely fast gas exchange $^{13}\text{C}_{T, \text{dis}}^* \xrightarrow{k_0 \rightarrow \infty} 0$.

Considering the different effects incorporated in the individual model experiments we write

$$\begin{aligned} ^{13}\text{C}_{\text{DIC, std}} &= ^{13}\text{C}_{\text{bio}} + ^{13}\text{C}_{\text{bio, std}}^* + ^{13}\text{C}_{T, \text{eq}}^* + ^{13}\text{C}_{T, \text{dis, std}}^* \\ ^{13}\text{C}_{\text{DIC, no-bio}} &= ^{13}\text{C}_{\text{bio}} + ^{13}\text{C}_{T, \text{eq}}^* + ^{13}\text{C}_{T, \text{dis, std}}^* \\ ^{13}\text{C}_{\text{DIC, fast-gasx-only}} &= ^{13}\text{C}_{\text{bio}} + ^{13}\text{C}_{T, \text{eq}}^* + ^{13}\text{C}_{T, \text{dis, fast}}^* \\ ^{13}\text{C}_{\text{DIC, inf-gasx-only}} &= ^{13}\text{C}_{\text{bio}} + ^{13}\text{C}_{T, \text{eq}}^* \\ ^{13}\text{C}_{\text{DIC, no-gasx}} &= ^{13}\text{C}_{\text{bio}} \\ ^{13}\text{C}_{\text{DIC, cons-gasx}} &= ^{13}\text{C}_{\text{bio}} + ^{13}\text{C}_{\text{bio, std}}^* \\ ^{13}\text{C}_{\text{DIC, fast-gasx}} &= ^{13}\text{C}_{\text{DIC, bio-fast}} = ^{13}\text{C}_{\text{bio}} + ^{13}\text{C}_{\text{bio, fast}}^* + ^{13}\text{C}_{T, \text{eq}}^* + ^{13}\text{C}_{T, \text{dis, fast}}^* \end{aligned} \quad (27)$$

This set of Eq. (27) provides a strategy to calculate the individual terms on the right-hand side using the sensitivity experiments:

$$\delta^{13}\text{C}_{T, \text{dis, fast}}^* \simeq \delta^{13}\text{C}_{\text{DIC, fast-gasx-only}} - \delta^{13}\text{C}_{\text{DIC, inf-gasx-only}} \quad (28)$$

$$\delta^{13}\text{C}_{T, \text{dis, std}}^* \simeq \delta^{13}\text{C}_{\text{DIC, no-bio}} - \delta^{13}\text{C}_{\text{DIC, inf-gasx-only}} \quad (29)$$

$$\begin{aligned} \delta^{13}\text{C}_{\text{bio, fast}}^* &\simeq \delta^{13}\text{C}_{\text{DIC, bio-fast}} - \delta^{13}\text{C}_{\text{DIC, fast-gasx-only}} \\ &\quad - \Delta\delta^{13}\text{C}_{\text{bio}} \end{aligned} \quad (30)$$

$$\delta^{13}\text{C}_{\text{bio, std}}^* \simeq \delta^{13}\text{C}_{\text{DIC, const-gasx}} - \delta^{13}\text{C}_{\text{DIC, no-gasx}}. \quad (31)$$

Equations (28)–(31) are approximations, assuming that delta values are conserved in addition/subtraction, which, as we have discussed above, is not generally the case. Exact expressions analogous to Eqs. (15), (16), and (19) are not possible since the total carbon expressions corresponding to the individual $^{13}\text{C}^*$ components are unknown. We will evaluate the errors caused with this assumption for some cases below.

5 Results

Analysis of various sensitivity tests in the preindustrial model is aimed at separating the influence of different processes (Sect. 5.1). This is followed by a detailed comparison of the late 20th century transient simulation of the standard model and model FeL with observations (Sect. 5.2).

5.1 Preindustrial simulations

5.1.1 Sea surface

Model *std* shows surface values of $\delta^{13}\text{C}_{\text{DIC}}$ (with $\delta^{13}\text{C}_{\text{CO}_2, \text{atm}}$ fixed at -6.5‰) ranging from less than 1‰ around Antarctica up to more than 2.6‰ in the tropics with largest meridional gradients (1.5‰) across the Southern Ocean (Figs. 3 and 4). This pattern is influenced by both biology and air–sea gas exchange. Biological effects ($\delta^{13}\text{C}_{\text{bio}}$) are well represented by $\Delta\delta^{13}\text{C}_{\text{bio}}$ estimates, which are consistent for both *std* and *fast-gasx* models with minor differences between the two around Antarctica (Fig. 4, top right panel). They lead to lower values in the Southern Ocean (-2‰), in the subarctic northwest Pacific (-1.5‰), in the Arctic and northern North Atlantic ($\sim -0.5\text{‰}$), and in the tropical regions of upwelling in the eastern parts of the ocean basins ($\sim 0.2\text{‰}$) and higher values in the subtropics ($\sim 0.6\text{‰}$). The areas with relatively low $\delta^{13}\text{C}$ are generally associated with regions of incomplete nutrient utilization. Model *FeL* shows somewhat smoother gradients in the tropical Pacific compared with *std* (Fig. 3).

Equilibrium fractionation alone in the case of infinitely fast air–sea gas exchange (*inf-gasx-only*) generates meridional gradients opposing those of biology, due to the temperature-dependent fractionation (Eq. 5), which depletes $\delta^{13}\text{C}_{\text{DIC}}$ by about 1‰ for every 10°C of warming (Broecker and Maier-Reimer, 1992) and leads to almost 3‰ differences between the equator and high latitudes. Model *fast-gasx-only* approximates that limit, but predicts somewhat smaller meridional gradients due to finite gas exchange, leading to minima of 1.4‰ at low latitudes and maxima of 3.7‰ at high latitudes (Fig. 4, top left panel). However, because of the slow air–sea equilibration time ($\sim 10\text{ yr}$) of surface waters with respect to $\delta^{13}\text{C}_{\text{DIC}}$ – the surface ocean is nowhere

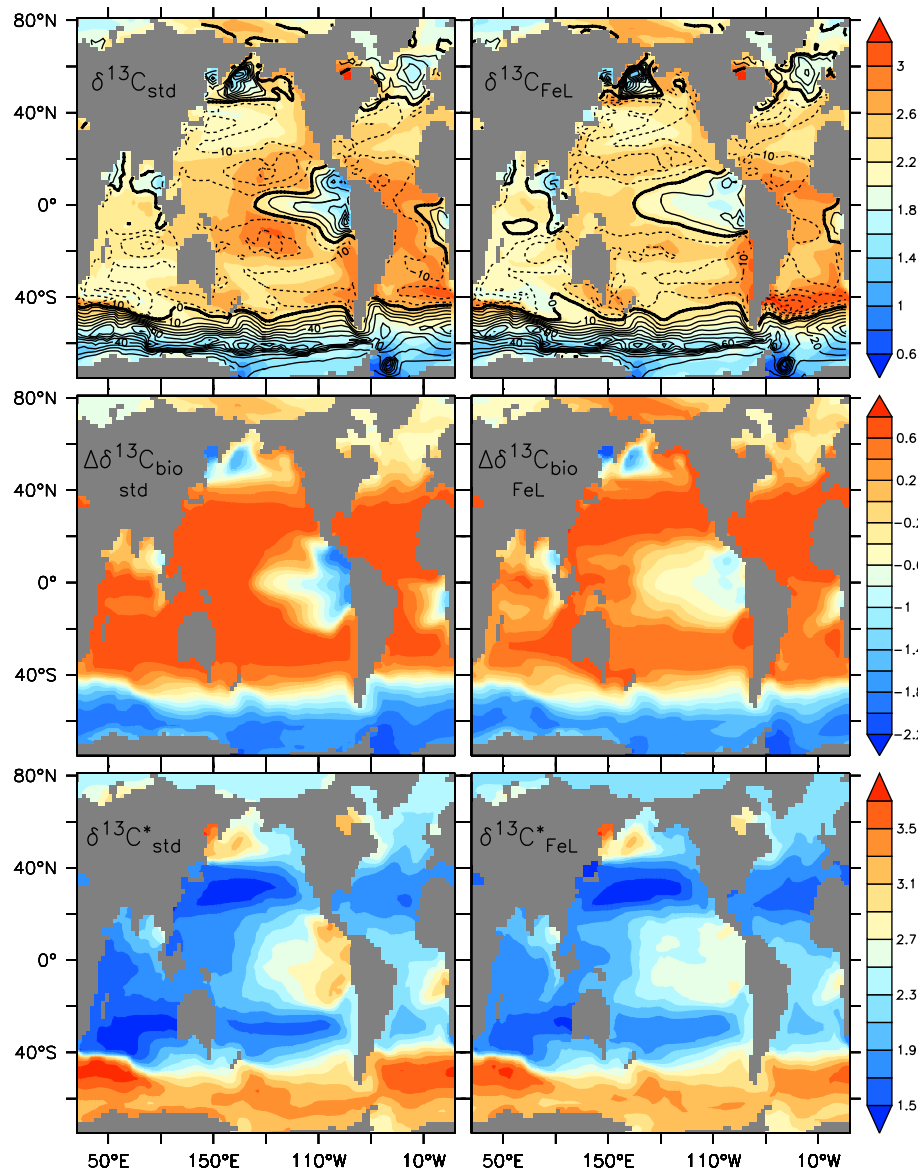


Fig. 3. Preindustrial surface $\delta^{13}\text{C}_{\text{DIC}}$ (top; color) and air–sea flux difference $\Delta F_{13\text{C}}$ (contour lines; positive downward negative values dashed), $\Delta\delta^{13}\text{C}_{\text{bio}}$ (center), and $\delta^{13}\text{C}^*$ (bottom) as a function of longitude and latitude for the standard model (*std*; left) and model *FeL* (right). In these experiments $\delta^{13}\text{C}$ of atmospheric CO_2 is fixed at -6.5‰ .

in equilibrium with the atmosphere (Lynch-Stieglitz et al., 1995) – the temperature-dependent air–sea gas exchange effect in model *std* ($\delta^{13}\text{C}_{T,\text{std}}^*$) is much reduced (*no-bio* versus *fast-gasx-only*) and has less impact on surface ocean $\delta^{13}\text{C}_{\text{DIC}}$ than biology. The reduced temperature-dependent air–sea gas exchange effect in model *std* is also apparent in the larger disequilibrium gradients $\delta^{13}\text{C}_{T,\text{dis},\text{std}}^*$ compared with $\delta^{13}\text{C}_{T,\text{dis},\text{fast}}^*$ (Fig. 4, bottom right). The effect of air–sea gas exchange acting on biological gradients in the standard model $\delta^{13}\text{C}_{\text{bio},\text{std}}^*$ increases $\delta^{13}\text{C}_{\text{DIC}}$ in the Southern Ocean but has little effects elsewhere (Fig. 4, top right). This effect is more efficient if gas exchange is faster and almost erases

the biological gradients in model *fast-gasx*. Meridional gradients of $\sim 1.5\text{‰}$ created by this effect are amplified by the thermodynamic gradients of $\sim 2.5\text{‰}$ to result in $> 4\text{‰}$ gradients created by air–sea gas exchange in model *fast-gasx* ($\delta^{13}\text{C}_{\text{fast}}^*$, Fig. 4, bottom right). The effect of air–sea gas exchange on surface ocean $\delta^{13}\text{C}_{\text{DIC}}$ in the standard model ($\delta^{13}\text{C}_{\text{std}}^*$) is much reduced, resulting in meridional gradients of $\sim 1.5\text{‰}$.

Slow air–sea gas exchange in the standard model leads to biological effects dominating the preindustrial surface ocean $\delta^{13}\text{C}_{\text{DIC}}$ distribution. This conclusion is supported by (a) a high positive correlation coefficient ($r = 0.75$) of

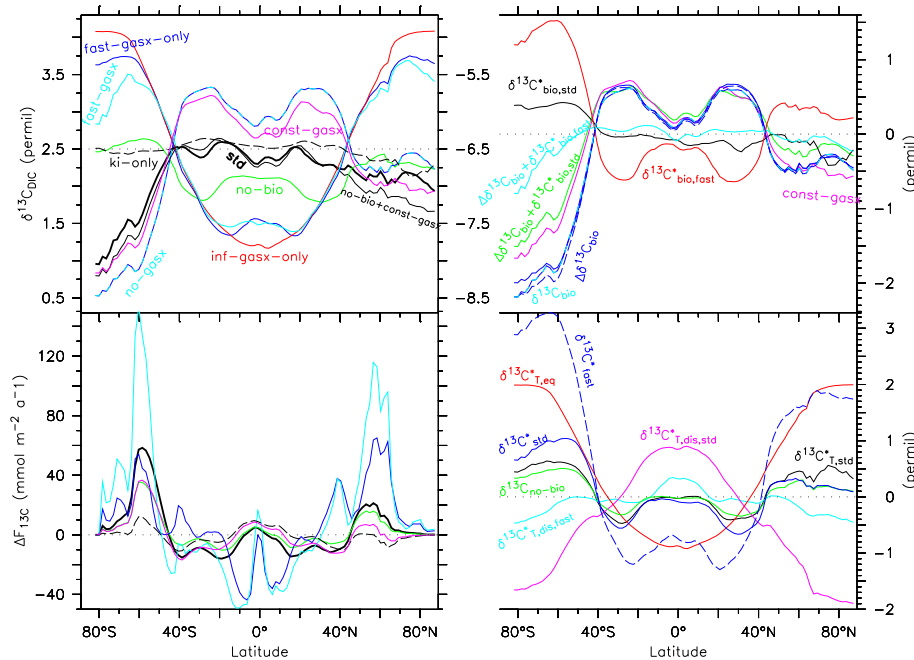


Fig. 4. Left panels: zonally averaged preindustrial surface $\delta^{13}\text{C}_{\text{DIC}}$ (top) and $\Delta F_{13\text{C}}$ (bottom) as a function of latitude for model *std* (thick black) and some of the sensitivity experiments listed in Table 1. Experiments *const-gasx* and *ki-only* use the right axis, all other experiments the left axis. The sparsely dotted line indicates the value of atmospheric $\delta^{13}\text{C}_\text{A} = -6.5\text{‰}$ (right axis). The curve for experiment *bio-fast* is identical to that of *fast-gasx*. The red curve labeled *inf-gasx-only* represents the equilibrium fractionation for infinitely fast gas exchange and has been calculated as described in the text. The thin black line has been calculated as $\delta^{13}\text{C}_{\text{DIC,no-bio}} + \delta^{13}\text{C}_{\text{DIC,const-gasx}} + 6.5\text{‰}$ and its difference with *std* indicates errors in the factorial analysis due to non-linearities. Right panels: effects of biological fractionation and air–sea gas exchange on surface $\delta^{13}\text{C}_{\text{DIC}}$ calculated using Eqs. (27)–(31). Top: $\Delta\delta^{13}\text{C}_{\text{bio}}$ (blue) from the standard model (Eq. 20, solid) and from model *bio-fast* (dashed), estimates of $\Delta\delta^{13}\text{C}_{\text{bio}} + \delta^{13}\text{C}_{\text{bio, std}}^*$ from $\delta^{13}\text{C}_{\text{DIC,const-gasx}}$ (purple) and from the difference $\delta^{13}\text{C}_{\text{DIC,std}} - \delta^{13}\text{C}_{\text{DIC,no-bio}}$ (green), $\Delta\delta^{13}\text{C}_{\text{bio}} + \delta^{13}\text{C}_{\text{bio, fast}}^*$ estimated from the difference $\delta^{13}\text{C}_{\text{DIC,bio-fast}} - \delta^{13}\text{C}_{\text{DIC,fast-gasx-only}}$ (light blue), $\delta^{13}\text{C}_{\text{bio, std}}^*$ estimated from $\delta^{13}\text{C}_{\text{DIC,const-gasx}} - \delta^{13}\text{C}_{\text{DIC,no-bio}}$ (black; mean subtracted), $\delta^{13}\text{C}_{\text{bio, fast}}^*$ calculated from $\delta^{13}\text{C}_{\text{DIC,bio-fast}} - \delta^{13}\text{C}_{\text{DIC,fast-gasx-only}} - \Delta\delta^{13}\text{C}_{\text{bio}}$ (red). Bottom: $\delta^{13}\text{C}_{\text{std}}^*$ (blue solid, Eq. 19), $\delta^{13}\text{C}_{\text{fast}}^*$ (blue dashed), $\delta^{13}\text{C}_{\text{T,eq}}^* = \delta^{13}\text{C}_{\text{DIC,inf-gasx-only}}$ (red; mean subtracted), $\delta^{13}\text{C}_{\text{T,dis,std}}^* + \delta^{13}\text{C}_{\text{DIC,no-bio}}$ (green) and $\delta^{13}\text{C}_{\text{DIC,std}} - \delta^{13}\text{C}_{\text{DIC,const-gasx}}$ (black; mean subtracted), $\delta^{13}\text{C}_{\text{T,dis,fast}}^*$ estimated from $\delta^{13}\text{C}_{\text{DIC,fast-gasx-only}} - \delta^{13}\text{C}_{\text{T,eq}}^*$ (light blue), and $\delta^{13}\text{C}_{\text{T,dis,std}}^*$ estimated from $\delta^{13}\text{C}_{\text{DIC,no-bio}} - \delta^{13}\text{C}_{\text{T,eq}}^*$ (purple). Vertical axes for the upper panels have the same lengths.

the spatial (horizontal) variability of surface $\delta^{13}\text{C}_{\text{DIC, std}}$ with $\Delta\delta^{13}\text{C}_{\text{bio}}$, whereas the correlation between $\delta^{13}\text{C}_{\text{DIC, std}}$ and $\delta^{13}\text{C}_{\text{std}}^*$ is much smaller and negative ($r = -0.35$); and (b) smaller spatial (horizontal) variability of $\delta^{13}\text{C}_{\text{std}}^*$ ($\sigma = 0.61\text{‰}$) versus that of $\Delta\delta^{13}\text{C}_{\text{bio}}$ ($\sigma = 0.84\text{‰}$). Nevertheless, air–sea gas exchange cannot be neglected; it strongly reduces the biologically created gradients ($\Delta\delta^{13}\text{C}_{\text{bio}}$ vs. $\delta^{13}\text{C}_{\text{DIC, std}}$).

In the standard model, air–sea fluxes ($\Delta F_{13\text{C}}$, Fig. 3 top left and Fig. 4 bottom left) tend to increase $\delta^{13}\text{C}_{\text{DIC}}$ at high latitudes and in the tropics, whereas they tend to decrease $\delta^{13}\text{C}_{\text{DIC}}$ in the subtropics and at mid-latitudes. Experiments *const-gasx* and *no-bio* both have attenuated fluxes compared with *std*, indicating that both biology and fractionation during air–sea gas exchange are similarly important in setting air–sea fluxes in *std*. Fast gas exchange modifies the pattern

such that air–sea fluxes north and south of the equator are now acting to strongly decrease surface $\delta^{13}\text{C}_{\text{DIC}}$, whereas mid-latitude fluxes tend to increase $\delta^{13}\text{C}_{\text{DIC}}$. The isotopic effects of air–sea fluxes are greatest in the case with biology and fast gas exchange (*fast-gasx*) because of the larger gradients imposed by biology that are counteracted by gas exchange.

Kinetic fractionation has only a minor effect on surface $\delta^{13}\text{C}_{\text{DIC}}$ patterns (*ki-only*). At fast gas exchange (*fast-gasx* minus *bio-fast*) kinetic fractionation leads to less than 0.05‰ higher values of surface–ocean $\delta^{13}\text{C}_{\text{DIC}}$ in the eastern equatorial Pacific and Atlantic and variations of less than $\pm 0.01\text{‰}$ elsewhere (not shown).

We conclude that the preindustrial surface $\delta^{13}\text{C}_{\text{DIC}}$ patterns are dominated by biology but that they are also markedly influenced by air–sea gas exchange, which

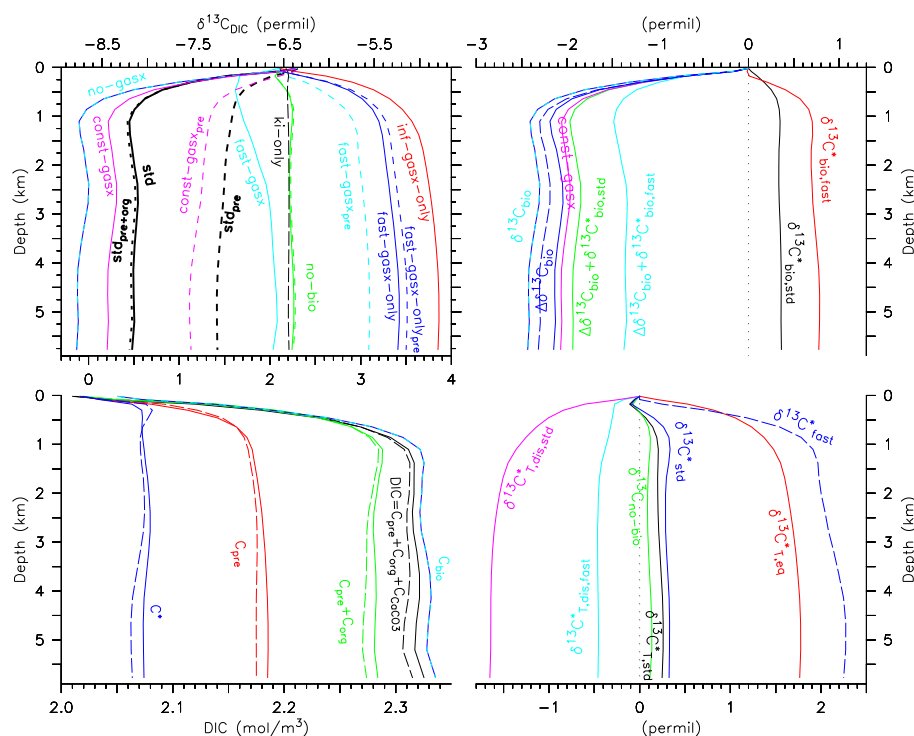


Fig. 5. Horizontally averaged vertical distribution of variables from preindustrial simulations. Top left: $\delta^{13}\text{C}_{\text{DIC}}$ (solid) and $\delta^{13}\text{C}_{\text{pre}}$ (dashed) for model *std* and some of the sensitivity experiments listed in Table 1. Experiments *const-gasx* and *ki-only* use the top axis, all other experiments the bottom axis. The curve for experiment *bio-equil* is identical to *fast-gasx*. The contributions from preformed plus organic ($\delta^{13}\text{C}_{\text{pre}}^{12}\text{C}_{\text{pre}} + \delta^{13}\text{C}_{\text{org}}^{12}\text{C}_{\text{org}}$)/($^{12}\text{C}_{\text{pre}} + ^{12}\text{C}_{\text{org}}$) for *std* is shown as the dotted thick black line. The difference between that line and $\delta^{13}\text{C}_{\text{DIC},\text{std}}$ (solid) represents the effect of CaCO_3 dissolution. Labeling is the same as in the top left panel of Fig. 4. Bottom left: DIC (black), $^{12}\text{C}_{\text{pre}}$ (red), $^{12}\text{C}_{\text{pre}} + ^{12}\text{C}_{\text{org}}$ (green), C^* (blue) from models *std* (solid) and *fast-gasx* (dashed), and C_{bio} from model *no-gasx* (light and dark blue dashed). Right panels: effects of biological fractionation and air–sea gas exchange on horizontally averaged $\delta^{13}\text{C}_{\text{DIC}}$ expressed as anomalies from surface values. Labeling is the same as in the right-hand panels of Fig. 4.

decreases the spatial gradients put into place by biology. This is in contrast to the conclusions of Broecker and Maier-Reimer (1992) that the “temperature influence largely compensates” the biological influence, and the conclusion by Gruber et al. (1999) that “biological effects on $\delta^{13}\text{C}$ nearly offset thermodynamic effects”, which were based on the analysis of anthropogenically contaminated observations.

Our conclusion also differs from that of MS00 who suggest that the primary factor controlling surface ocean $\delta^{13}\text{C}_{\text{DIC}}$ distributions is the wind speed-dependent gas transfer velocity and that biology is a secondary factor, although their statement refers perhaps more to the potential effect of fast air–sea gas exchange, which can be larger than the biological influence.

As we will show below, the intrusion of isotopically light anthropogenic $\delta^{13}\text{C}_{\text{DIC}}$ reduces spatial gradients in the surface ocean. Thus transient penetration of anthropogenic carbon into near-surface ocean may have led to the false impression of a compensation between temperature and biological effects, whereas in the preindustrial surface ocean the

biological influence may have dominated spatial variability in $\delta^{13}\text{C}_{\text{DIC}}$ as our model experiments suggest.

5.1.2 Ocean interior

In the plots of vertical distributions of $\delta^{13}\text{C}_{\text{DIC}}$ (Fig. 5), values from the various model sensitivity tests converge approximately at the sea surface. This is an effect of running the model with a fixed atmospheric $\delta^{13}\text{C}$. In the real world, keep in mind that the carbon isotope budget of the combined atmosphere–ocean system is largely controlled by the dominant dissolved inorganic carbon reservoir in the deep sea. If the global rather than atmospheric budget of ^{13}C had been fixed, the deep ocean values would approximately converge, and the major divergence between model runs would be in the near-surface ocean and atmosphere.

Model *std* shows nearly constant values of globally horizontally averaged $\delta^{13}\text{C}_{\text{DIC}} = 0.5\text{‰}$ below 1 km, whereas above that depth $\delta^{13}\text{C}_{\text{DIC}}$ rises rapidly to 2.2‰ at the surface (0–100 m) leading to a surface-to-deep gradient of -1.7‰ (Fig. 5, top left). About -0.8‰ of that gradient in model *std* is caused by the advection of low $\delta^{13}\text{C}_{\text{pre}}$ from high

latitudes, particularly from the Southern Ocean, whereas about -0.9‰ is due to the remineralization of isotopically light organic matter ($\delta^{13}\text{C}_{\text{org}}$). These contributions correspond to the roughly equal contributions of preformed and remineralized carbon to the surface-to-deep DIC gradient (Fig. 5, bottom left). The calcium carbonate cycle has only a minor effect and increases deep ocean $\delta^{13}\text{C}_{\text{DIC}}$ by 0.03‰ (difference between thick dotted and solid black lines in top left panel of Fig. 5). This effect is small because (a) the smaller relative contribution ($\sim 15\%$) of the carbonate pump on surface-to-deep ocean DIC gradients (difference between green and black solid lines in bottom left panel of Fig. 5) and (b) the small difference in $\delta^{13}\text{C}$ between calcium carbonate and deep ocean DIC (only $\sim 1.5\text{‰}$ in contrast to $\sim 20\text{‰}$ for organic carbon).

Biological fractionation alone leads to large surface-to-deep gradients of -2.3‰ (*no-gasx*, $\delta^{13}\text{C}_{\text{bio}}$, Fig. 5, top), which is slightly underestimated by $\Delta\delta^{13}\text{C}_{\text{bio}}$ (-2.1‰). (Nevertheless, $\Delta\delta^{13}\text{C}_{\text{bio}}$ is a good approximation for the three-dimensional distribution of $\delta^{13}\text{C}_{\text{bio}}$ as indicated by their high correlation coefficient $r > 0.99$.) The potential thermal effect of equilibrium fractionation alone in the case of infinitely fast gas exchange (*inf-gasx-only*; Fig. 5 top left), on the other hand, would lead to 1.6‰ higher $\delta^{13}\text{C}_{\text{DIC}}$ values in the deep ocean than at the surface. (Model *fast-gasx-only* approaches that limit, but due to the still finite gas exchange, it predicts a somewhat smaller surface-to-deep $\delta^{13}\text{C}_{\text{DIC}}$ gradient of 1.2‰ .) Slow air–sea gas exchange, however, limits the thermodynamic effect such that the vertical gradient is reduced to almost 0‰ in experiment *no-bio*, consistent with the results of MS00 (their “Solubility Model”). Note that changes in air–sea gas exchange do not modulate significantly the impact of remineralized carbon on deep ocean $\delta^{13}\text{C}_{\text{DIC}}$, which is $\sim 1\text{‰}$ in all cases with biological fractionation (differences between dashed and corresponding solid lines in top left panel of Fig. 5).

Model *const-gasx* as well as the difference *std* – *no-bio* (green line in top right panel of Fig. 5) display consistently slightly smaller vertical gradients than $\delta^{13}\text{C}_{\text{bio}}$ and $\Delta\delta^{13}\text{C}_{\text{bio}}$, indicating the small but significant (0.1 – 0.5‰) moderating effect of non-fractionating gas exchange on biologically created vertical gradients ($\delta^{13}\text{C}_{\text{bio, std}}^*$). This non-fractionating gas exchange effect is stronger ($\sim 0.7\text{‰}$) in the case of fast gas exchange ($\delta^{13}\text{C}_{\text{bio, fast}}^*$) and conspires with the reduced disequilibrium thermodynamic effect $\delta^{13}\text{C}_{T, \text{dis, fast}}^*$ (bottom right panel of Fig. 5) to generate small vertical gradients in model *fast-gasx* (top left panel, Fig. 5).

In model *std*, however, the disequilibrium thermodynamic effect cancels almost entirely the equilibrium thermodynamic effect (black and green lines in bottom right panel of Fig. 5). Together with the small effect of $\delta^{13}\text{C}_{\text{bio, std}}^*$ this causes the overall effect of air–sea gas exchange to increase deep ocean values by $\sim 0.3\text{‰}$ with respect to the surface ($\delta^{13}\text{C}_{\text{std}}^*$). Fast gas exchange, in contrast, increases deep

ocean values by more than 2‰ with respect to the surface ($\delta^{13}\text{C}_{\text{fast}}^*$).

The effects of kinetic fractionation (*ki-only*) on deep ocean $\delta^{13}\text{C}_{\text{DIC}}$ are negligibly small. In model *fast-gasx-only*, although biological fractionation is zero, the sinking of organic matter and calcium carbonate delivers the surface $\delta^{13}\text{C}_{\text{DIC}}$ signature to the deep ocean, reducing vertical gradients by 0.1‰ (dashed vs. solid blue lines in top left panel of Fig. 5). This effect is weaker in model *no-bio* since vertical gradients in $\delta^{13}\text{C}_{\text{DIC}}$ are weaker.

In model *std* zonally averaged preindustrial $\delta^{13}\text{C}_{\text{DIC}}$ in the deep ocean varies from 1.6‰ in the North Atlantic to -0.2‰ in the North Pacific (Fig. 6). The spatial variability in the deep ocean is dominated by 2.0‰ variations of $\Delta\delta^{13}\text{C}_{\text{bio}}$, decreasing from -0.7‰ in the North Atlantic to -2.7‰ in the North Pacific, whereas $\delta^{13}\text{C}^*$ variations are smaller (0.5‰) and increase from 2.2‰ in the North Atlantic to 2.7‰ in the Southern Ocean. A pronounced maximum of $\delta^{13}\text{C}^*$ is simulated in Antarctic Intermediate Water (AAIW) in the Atlantic with values ranging from 3‰ at high latitudes to $\sim 2.4\text{‰}$ in the tropics, consistent with estimates based on observations (Charles et al., 1993). Remineralized isotope signature ($\Delta\delta^{13}\text{C}_{\text{rem}} = \delta^{13}\text{C}_{\text{DIC}} - \delta^{13}\text{C}_{\text{pre}}$) variations are similar to those of $\Delta\delta^{13}\text{C}_{\text{bio}}$ except in the Atlantic, where they are smaller, whereas absolute values of $\Delta\delta^{13}\text{C}_{\text{rem}}$ are higher than $\Delta\delta^{13}\text{C}_{\text{bio}}$. Most of the differences between $\Delta\delta^{13}\text{C}_{\text{bio}}$ and $\Delta\delta^{13}\text{C}_{\text{rem}}$ (and between $\delta^{13}\text{C}^*$ and $\delta^{13}\text{C}_{\text{pre}}$) can be explained by preformed nutrients, which are higher in Southern Ocean deep and intermediate water masses and lower in North Atlantic Deep Water (NADW) and exhibit larger variability in the deep Atlantic compared to the Indo-Pacific (Ito and Follows, 2005; Schmittner and Galbraith, 2008). $\delta^{13}\text{C}_{\text{pre}}$ variations are much smaller and decrease by $\sim 0.4\text{‰}$ from the North Atlantic towards the North Pacific. In the thermocline the variability of $\delta^{13}\text{C}_{\text{pre}}$ is larger (1‰), reflecting more the surface variations (Fig. 3).

Individual contributions to $\delta^{13}\text{C}^*$ are shown in Fig. 7. By definition $\delta^{13}\text{C}_{T, \text{eq}}^*$ depends only on temperature and varies from $\sim 1\text{‰}$ in the tropical surface ocean to $\sim 3.8\text{‰}$ in the abyss and high latitude surface waters. Due to large disequilibrium effects caused by the slow air–sea gas exchange these variations are only weakly expressed in $\delta^{13}\text{C}_{T, \text{std}}^*$, which shows minima of $\sim 1.6\text{‰}$ in subtropical surface waters and maxima of $\sim 2.7\text{‰}$ in surface waters of the Southern Ocean and northwest Pacific (not shown) and small variations ($\sim 0.2\text{‰}$) in the deep ocean. The non-fractionating effect of air–sea gas exchange acting on the biological gradients ($\delta^{13}\text{C}_{\text{bio, std}}^*$) leads to minima in the subtropical surface and maxima in AAIW and Antarctic Bottom Water. Thus the maximum in $\delta^{13}\text{C}^*$ in AAIW is caused in approximately equal parts by $\delta^{13}\text{C}_{T, \text{std}}^*$ and $\delta^{13}\text{C}_{\text{bio, std}}^*$. It is interesting to note that for fast gas exchange the AAIW maximum in $\delta^{13}\text{C}_{T, \text{fast}}^*$ is less pronounced than $\delta^{13}\text{C}_{T, \text{std}}^*$, whereas it is more pronounced in $\delta^{13}\text{C}_{\text{bio, fast}}^*$.

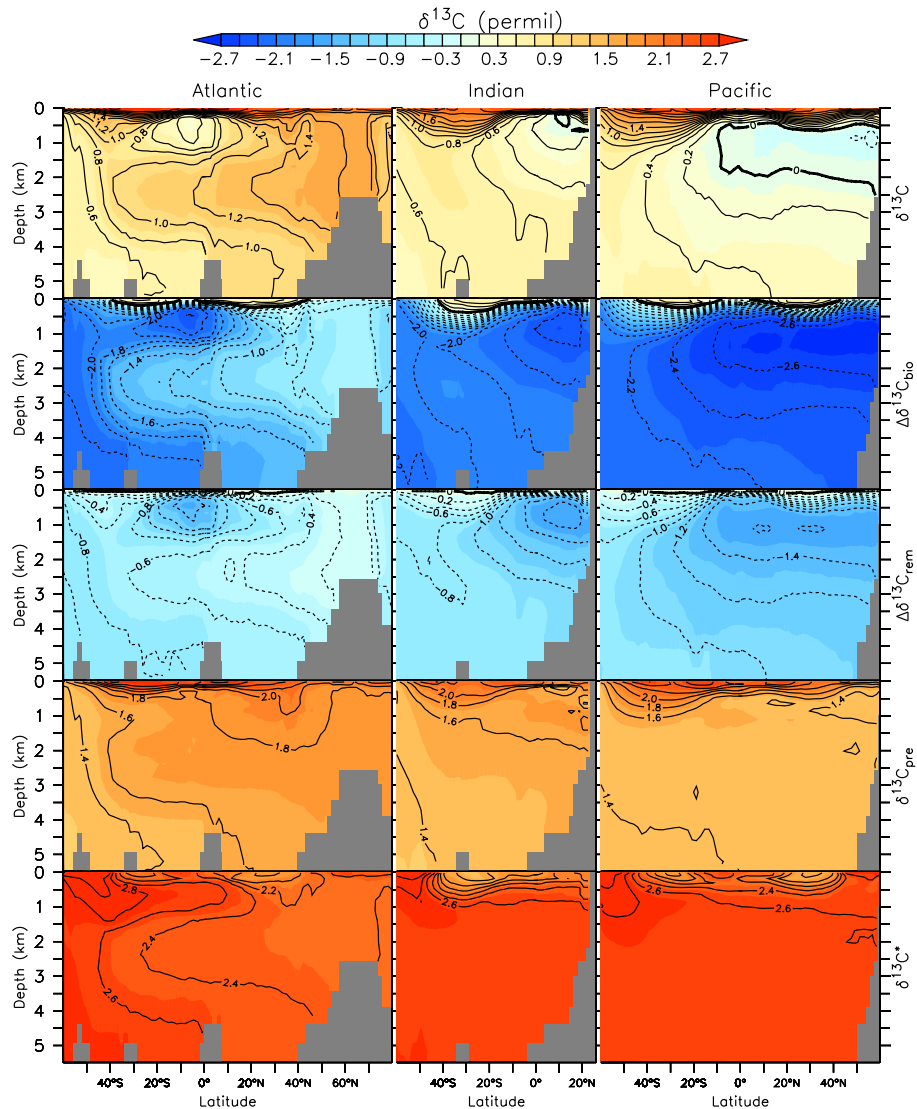


Fig. 6. Zonally averaged preindustrial $\delta^{13}\text{C}_{\text{DIC}}$ (top), $\Delta\delta^{13}\text{C}_{\text{bio}}$ (second from top), $\Delta\delta^{13}\text{C}_{\text{rem}}$ (center), $\delta^{13}\text{C}_{\text{pre}}$ (second from bottom), and $\delta^{13}\text{C}^*$ (bottom) in model *std* in the Atlantic (left), Indian (center) and Pacific (right) oceans.

We conclude from these preindustrial simulations that the vertical distribution of $\delta^{13}\text{C}_{\text{DIC}}$ in the ocean and the spatial gradients between deep water masses are dominated by the effects of biological fractionation, in agreement with previous studies (Broecker and Maier-Reimer, 1992; Lynch-Stieglitz et al., 1995; MS00). Air–sea gas exchange reduces the $\delta^{13}\text{C}_{\text{DIC}}$ gradients generated by biology by 10–20% in the pre-anthropogenic simulation. Under different climate regimes this fraction as well as the efficiency of gas exchange as a means of changing the preformed properties of water masses entering the ocean interior could be different.

5.2 Present day (1990–2005) observations and simulations

The modeled large-scale circulation and distribution of biogeochemical tracers is generally in good agreement with observations, although systematic biases remain. In the North Pacific, stratification is too weak, leading to anomalously high subsurface oxygen and low DIC and nutrient concentrations there. In the deep Indian Ocean, oxygen and radiocarbon are too high while DIC and nutrient concentrations are too low (Schmittner et al., 2008). The model does not include interactive iron and silicon cycles, which leads to biases in simulating phytoplankton growth rates. These known biases also affect the simulated $\delta^{13}\text{C}_{\text{DIC}}$ distribution, which we need to consider when comparing model results to observations.

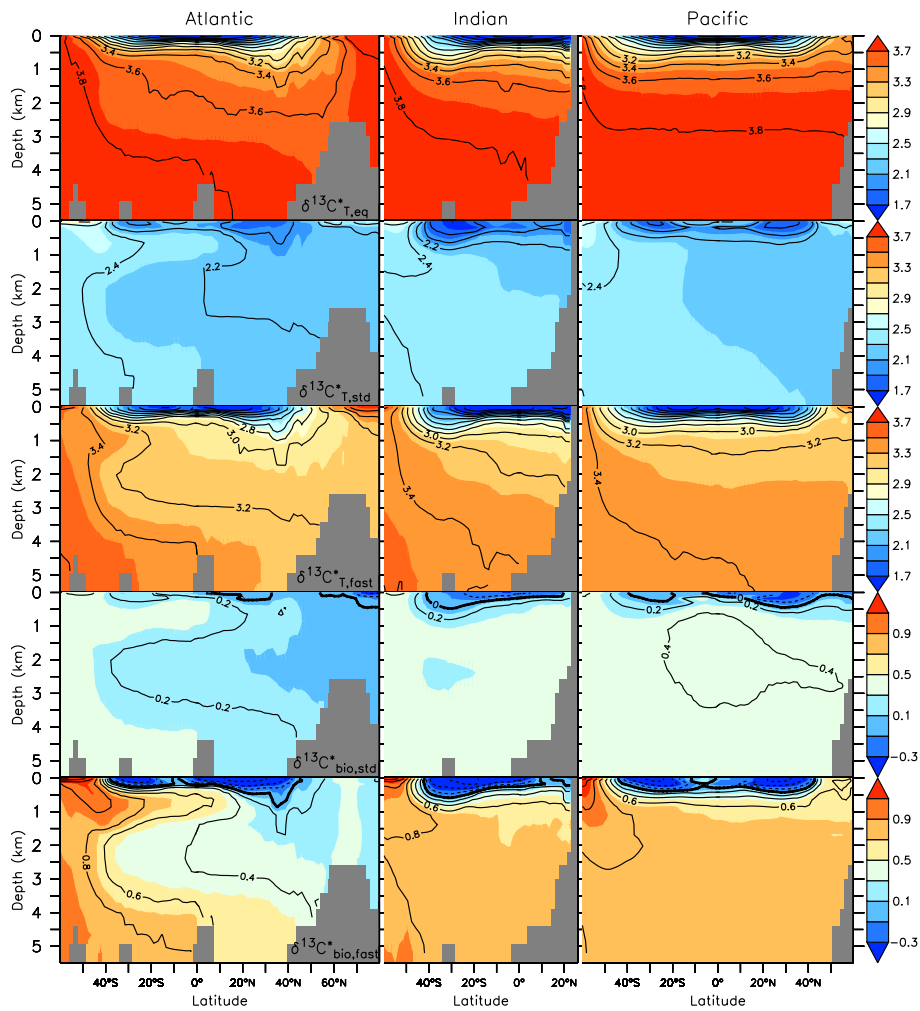


Fig. 7. As Fig. 6 but showing individual components of $\delta^{13}\text{C}^*$. From top $\delta^{13}\text{C}^*_{T,eq}$; $\delta^{13}\text{C}^*_{T,std}$; $\delta^{13}\text{C}^*_{T,fast}$; $\delta^{13}\text{C}^*_{bio,std}$ (global surface mean subtracted); $\delta^{13}\text{C}^*_{bio,fast}$. Note that the color scale for the top three rows is different from the bottom two.

In this section annual mean values will be used for all data unless specified otherwise.

5.2.1 Particulate organic matter

Figure 8 compares model results to the compilation of measurements of $\delta^{13}\text{C}$ in particulate organic matter (POM) in the near-surface ocean by Goericke and Fry (1994). Particulate organic carbon is about 2‰ lower in the 1990s compared with the preindustrial simulation due to both the decrease of surface-ocean $\delta^{13}\text{C}_{\text{DIC}}$ and an increase in the $p\text{CO}_2$ -dependent fractionation (Eq. 7). Models *FeL* and *std* simulate very similar zonally averaged $\delta^{13}\text{C}_{\text{POC}}$ distributions. Both reproduce the observed general meridional gradient of $\delta^{13}\text{C}_{\text{POC}}$ with less negative values of about -20‰ at low latitudes and more negative values (-25 to -30‰) at high latitudes, similar to earlier studies (Hofmann et al., 2000; MS00). Correlation coefficients between model results and

observations of $r = 0.74$ (*FeL*), $r = 0.71$ (*std*) and normalized (by the standard deviation of the observations, which is $\sigma_{\text{obs}} = 2.8\text{‰}$) root mean squared errors are $\text{NRMSE} = 0.92$ (*FeL*) and $\text{NRMSE} = 0.98$ (*std*) suggest model *FeL* is in slightly better agreement with the observations than model *std*.

However, closer inspection reveals that model *FeL* underestimates $\delta^{13}\text{C}_{\text{POC}}$ in the eastern tropical Pacific (a bias that is exacerbated in model *std*; not shown), in the subarctic North Pacific and in the high-latitude North Atlantic. It is unable to reproduce the pronounced interhemispheric difference at mid- to high latitudes apparent in the observations; qualitatively similar biases occurred in the more complex model of Tagliabue and Bopp (2008).

Large gaps in the data coverage hamper a more comprehensive model validation at this time. An updated compilation of surface $\delta^{13}\text{C}_{\text{POC}}$ measurements and new measurements, particularly in the Pacific, are urgently required to

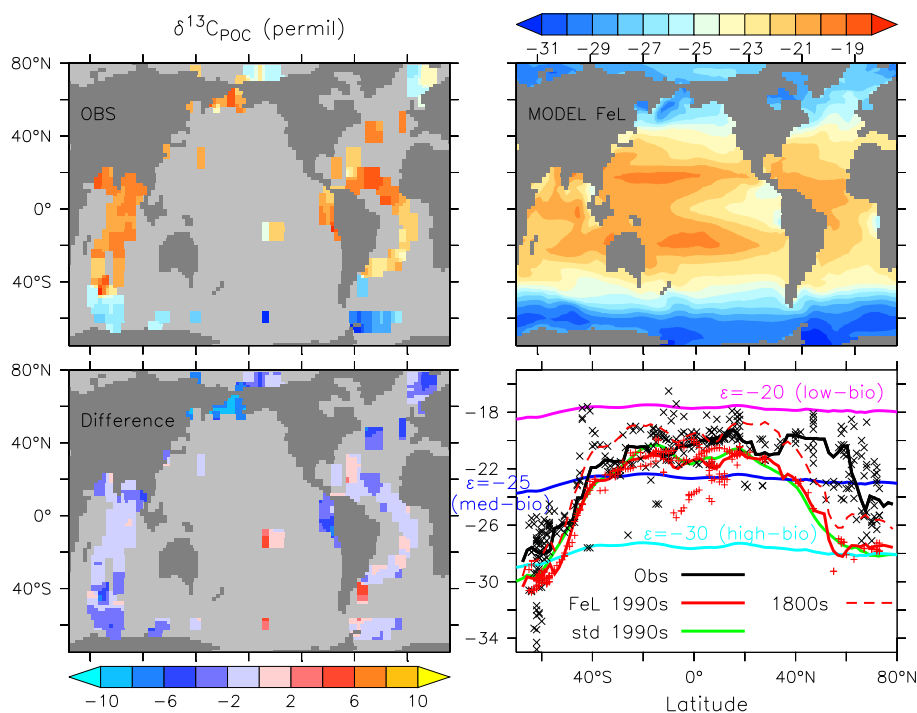


Fig. 8. $\delta^{13}\text{C}$ of particulate organic carbon (POC) from observations (Goericke and Fry, 1994) averaged on a 5° grid (top left) and model *FeL* (top right; 1990s averaged over the top 100 m) presented as longitude-latitude maps. Bottom left: difference model *FeL* minus observations. Bottom right: zonal averages as a function of latitude. Symbols show individual observations (black) and *FeL* model results (red) at the locations of the observations. Lines show zonal averages using grid points where observations are available only. Red dashed line represents results from the preindustrial *FeL* model simulation. Model *std* is shown in green; other models are *low-bio* (purple), *med-bio* (blue) and *high-bio* (light blue).

improve the validation of biological fractionation in global models. Surface sediment data may provide an alternative to sea surface $\delta^{13}\text{C}_{\text{POC}}$ measurements, a possibility that should be explored in the future.

Future improvements of the model will need to include a more realistic treatment of biological fractionation such as outlined in the approaches of Rau et al. (1996) and Keller and Morel (1999). This will likely require more ecosystem and nutrient information to constrain the relative growth rates and isotopic fractionation of different classes of plankton.

5.2.2 Surface dissolved inorganic carbon

The global mean surface $\delta^{13}\text{C}_{\text{DIC}}$ value from the 1990–2005 observations of 1.5‰ is slightly overestimated by the models *FeL* (1.6‰) and *std* (1.7‰). As noted earlier by Gruber et al. (1999), observations show that $\delta^{13}\text{C}_{\text{DIC}}$ is relatively constant over most of the surface ocean (Fig. 9); zonally averaged values range between 1 and 2‰ , although the total range of measured $\delta^{13}\text{C}_{\text{DIC}}$ values stretches between 0.5 and 2.4‰ . Larger simulated latitudinal gradients in surface-ocean $\delta^{13}\text{C}_{\text{DIC}}$ for preindustrial time (1 – 2.5‰ for zonally averaged values; Fig. 4) suggest that the measured gradients are reduced as a result of the accumulation of anthropogenic carbon into the tropical and subtropical oceans. An-

thropogenic carbon reduces the area-weighted spatial (horizontal) standard deviation of surface $\delta^{13}\text{C}_{\text{DIC}}$ from 0.37‰ at year 1800 to 0.27‰ at year 2000 in model *FeL*. The reduction in spatial variability is almost identical (0.36‰ in 1800 to 0.27‰ in 2000) in model *std*.

High surface $\delta^{13}\text{C}_{\text{DIC}}$ values are observed in the western equatorial Pacific, in the central Pacific south of the equator, in the southeast Pacific, in the tropical Atlantic and near the subantarctic front in the Southern Ocean. Low values are found in the Indian Ocean, the northeast Pacific, the central and eastern equatorial Pacific, the northwestern subtropical Pacific, the subtropical North Atlantic as well as at high latitudes. Model *FeL* captures many of the observed spatial patterns of surface ocean $\delta^{13}\text{C}_{\text{DIC}}$ with a correlation coefficient of $r = 0.53$ and $\text{NRMSE} = 0.99$. Zonally averaged $\delta^{13}\text{C}_{\text{DIC}}$ values in model *FeL* are generally consistent with observations except around 20°N and in the Arctic, where the model is biased high. However, model *std* ($r = 0.49$; $\text{NRMSE} = 1.19$) overestimates $\delta^{13}\text{C}_{\text{DIC}}$ in the tropics (by up to 0.4‰ and for the zonal average by 0.2 – 0.3‰) except for the eastern equatorial Pacific where $\delta^{13}\text{C}_{\text{DIC}}$ is underestimated (not shown, but see Fig. 3 for the differences with model *FeL* in preindustrial patterns). Including iron limitation reduces phytoplankton growth rates, carbon biomass,

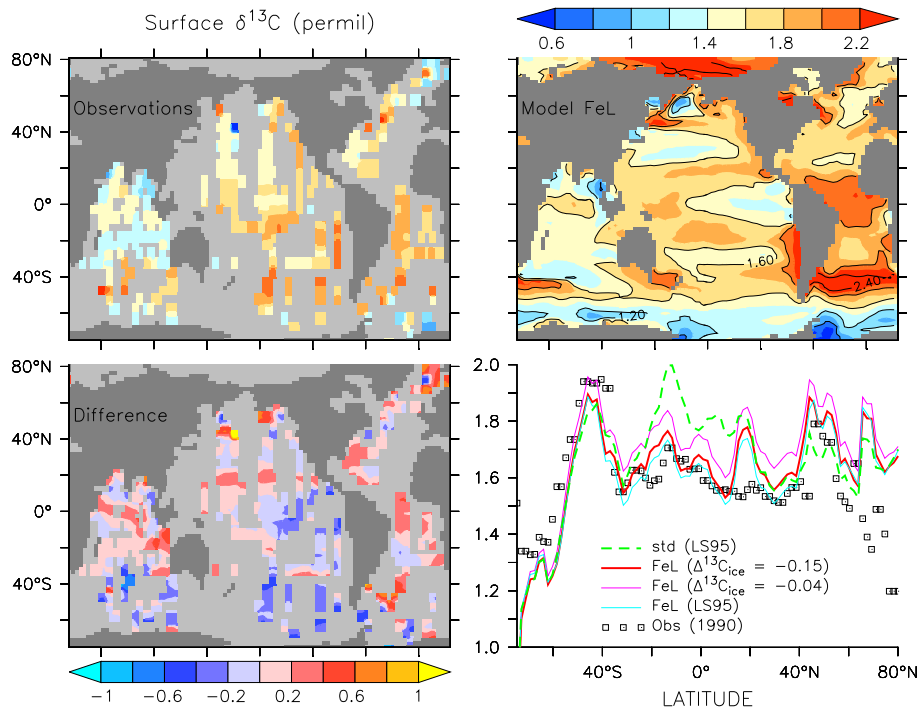


Fig. 9. Comparison of surface $\delta^{13}\text{C}_{\text{DIC}}$ distribution from observations of the 1990s (Gruber and Keeling, 2001; top left) and the model (1980–1999 average, top right). Bottom left: difference model minus observations. Bottom right: zonally averaged values as a function of latitude. Only those model grid boxes are considered in the averaging where corresponding observations exist. Square symbols show observations, the lines show models *std* (dashed green) and *FeL* (solid red, purple and light blue lines). The different solid lines explore the uncertainty due to the atmospheric $\delta^{13}\text{C}$ evolution and correspond to the same lines in Fig. 2

and hence primary productivity in the eastern equatorial Pacific (Fig. 1) and eliminates the bias in $\delta^{13}\text{C}_{\text{DIC}}$. This illustrates the importance of details of ecosystem model dynamics on the $\delta^{13}\text{C}$ distribution and suggests that $\delta^{13}\text{C}$ observations can help evaluate ocean ecosystem models.

Remaining biases in model *FeL* include overestimated surface-ocean $\delta^{13}\text{C}_{\text{DIC}}$ values in parts of the tropical Atlantic and Indian Ocean, along 20°N in the North Pacific, in the northern North Pacific and northern North Atlantic, and in the mid-latitude South Atlantic as well as underestimation of surface-ocean $\delta^{13}\text{C}_{\text{DIC}}$ in the Southern Ocean and eastern tropical Pacific.

The model suggests that preindustrial $\delta^{13}\text{C}_{\text{DIC}}$ values at the sea surface were, on a global average, 2.3‰, or 0.67‰ higher than in the 1990s, in agreement with the previous estimates by Broecker and Maier-Reimer (1992, 0.7‰ for the 1970s) and Sonnerup et al. (2007, 0.76 ± 0.12 ‰). Ortiz et al. (2000) calculated a shift of 0.62 ± 0.17 ‰ in the Northeast Pacific (using data from 1991), consistent with the model 1980–2000 mean between 138°W to 120°W and 28°N to 45°N of 0.75‰. Surface-ocean $\delta^{13}\text{C}_{\text{DIC}}$ decreases faster in the subtropics than at other latitudes consistent with previous analysis of observations (Quay et al., 2003). Between the 1980s and the 1990s its decrease ranges from minima

of ~ 0.04 ‰ at high latitudes to 0.2‰ in the subtropics, and ~ 0.14 ‰ in the tropics, consistent with previous studies (e.g. Gruber et al., 1999).

5.2.3 Ocean interior dissolved inorganic carbon

Global mean surface-to-deep gradients of 1.0‰ in the observations are well captured in both models (top left Fig. 10). This is a considerable reduction compared to the modeled preindustrial gradients of 1.7‰ (Fig. 8; Sect. 5.1.2), indicating that the invasion of isotopically light anthropogenic carbon decreased the vertical $\delta^{13}\text{C}_{\text{DIC}}$ gradient. Both models are biased high (globally by 0.09‰) particularly at mid-depths. A high bias is not uncommon. All models tested by Sonnerup and Quay (2012) and Tagliabue and Bopp (2008) were biased high (by 0.13–0.51‰ and more than 0.45‰ below 1 km depth, respectively; the numbers from Tagliabue and Bopp (2008) cannot be precisely compared with ours because they did not present volume weighted averages and used a much sparser dataset).

Model biases in deep ocean $\delta^{13}\text{C}_{\text{DIC}}$ are mirrored by similar biases of opposite sign in DIC (bottom left panel in Fig. 10), indicating that improving the DIC simulation would also lead to a better isotope distribution. Model *FeL* has lower $\delta^{13}\text{C}_{\text{DIC}}$ and higher DIC values in the deep ocean and at the

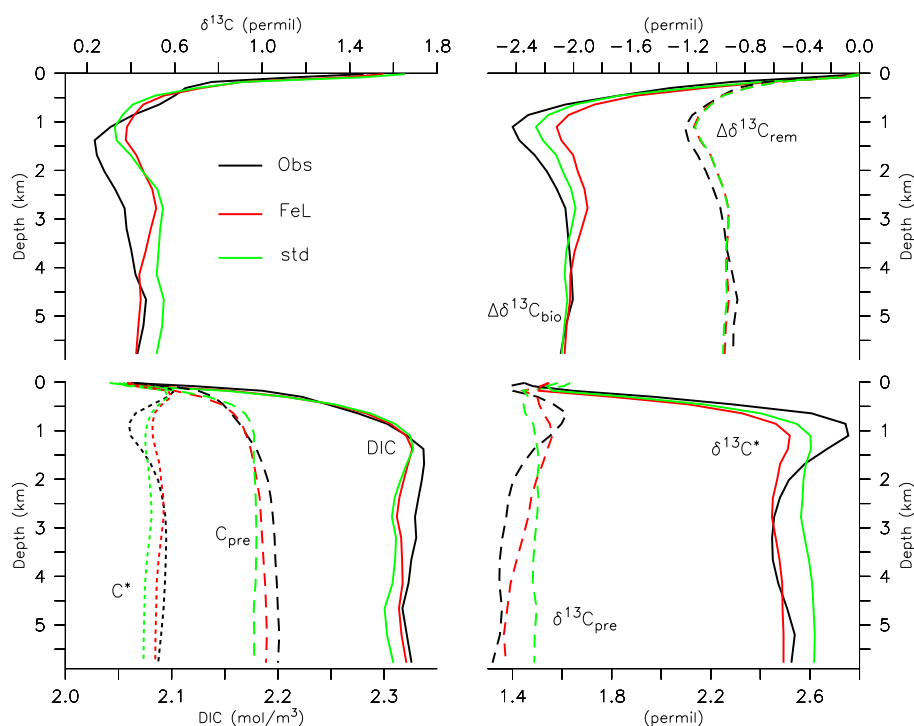


Fig. 10. As Fig. 5 but for the 1990s including observations (black) and models *FeL* (red) and *std* (green). Top left: $\delta^{13}\text{C}_{\text{DIC}}$. Top right: $\Delta\delta^{13}\text{C}_{\text{bio}}$ (solid) and $\Delta\delta^{13}\text{C}_{\text{rem}}$ (dashed). Bottom right: $\delta^{13}\text{C}^*$ (solid) and $\delta^{13}\text{C}_{\text{pre}}$ (dashed). Bottom left: DIC (solid), C_{pre} (dashed), and C^* .

surface compared with *std* and agrees better with observations there. Much of the overestimation of $\delta^{13}\text{C}_{\text{DIC}}$ and underestimation of DIC in the model's deep ocean is due to too low preformed carbon and too high $\delta^{13}\text{C}_{\text{pre}}$ there.

The average depth distributions of $\Delta\delta^{13}\text{C}_{\text{bio}}$, $\Delta\delta^{13}\text{C}_{\text{rem}}$, $\delta^{13}\text{C}_{\text{pre}}$, and $\delta^{13}\text{C}^*$ simulated by the models agree well with the observations (Fig. 10), confirming the conclusions drawn from the preindustrial model results above. Comparison with Fig. 5 shows that anthropogenic carbon has strongly decreased the vertical gradients in $\delta^{13}\text{C}_{\text{pre}}$ whereas it has increased $\delta^{13}\text{C}^*$ gradients. While vertical gradients in the preindustrial simulation are about twice as large for $\delta^{13}\text{C}_{\text{pre}}$ (0.6 ‰) than for $\delta^{13}\text{C}^*$ (0.3 ‰), contemporary gradients are much larger for $\delta^{13}\text{C}^*$ (1 ‰) than for $\delta^{13}\text{C}_{\text{pre}}$ (~ 0 ‰).

Spatial gradients in deep water $\delta^{13}\text{C}_{\text{DIC}}$ of about 1.6 ‰ are apparent between different ocean basins in both observations and in the model (Figs. 11, 12). Highest values of around 1 ‰ are found in the North Atlantic, whereas lowest values of less than -0.6 ‰ are found in the North Pacific at about 1 km depth, consistent with an earlier data compilation (Kroopnick, 1985). Model *FeL* ($r = 0.88$, $\text{NRMSE} = 0.50$; $\sigma_{\text{obs}} = 0.48$ ‰) captures the observed three-dimensional distribution slightly better than model *std* ($r = 0.85$, $\text{NRMSE} = 0.58$).

Most of the observed variability of $\delta^{13}\text{C}_{\text{DIC}}$ in the deep ocean is due to $\Delta\delta^{13}\text{C}_{\text{bio}}$ (Figs. 10, 11), which ranges from values close to -1 ‰ in the North Atlantic to -2.8 ‰ in

the North Pacific. Much of this variability is due to the effect of remineralized matter $\Delta\delta^{13}\text{C}_{\text{rem}}$, which ranges from -0.3 ‰ in the North Atlantic to -1.7 ‰ in the North Pacific. Observed $\delta^{13}\text{C}_{\text{pre}}$ shows little variability in the deep ocean but maxima in the thermocline in all ocean basins, particularly at low latitudes. Model results reproduce this pattern (Fig. 12) and indicate that large vertical gradients in preindustrial $\delta^{13}\text{C}_{\text{pre}}$ in the upper thermocline have been reduced due to the invasion of anthropogenic carbon (Figs. 10, 12 vs. Figs. 6 and 14). Higher preformed values of upper ocean and intermediate waters are consistent with the simulated preindustrial surface $\delta^{13}\text{C}_{\text{DIC}}$ distribution (Fig. 3), which shows lower values at high latitude regions of deep water formation and higher values in lower latitude regions of intermediate and mode water formation. For preindustrial times the model simulates a monotonic decrease of $\delta^{13}\text{C}_{\text{pre}}$ from the surface down (Fig. 6). Thus, the intermediate depth maximum simulated for the contemporary ocean is caused by the downward penetration of light carbon from above superimposed on this background gradient, suggesting that this is also the reason for the observed pattern.

The spatial gradients in observed $\delta^{13}\text{C}^*$ are larger than those for $\delta^{13}\text{C}_{\text{pre}}$ and show minima in the subtropical surface ocean of ~ 1 ‰ and maxima of up to 3 ‰ for AAIW. Pronounced differences are apparent between water masses of southern origin, which are high in $\delta^{13}\text{C}^*$ and NADW, which has lower values. Models *FeL* and *std* reproduce the general

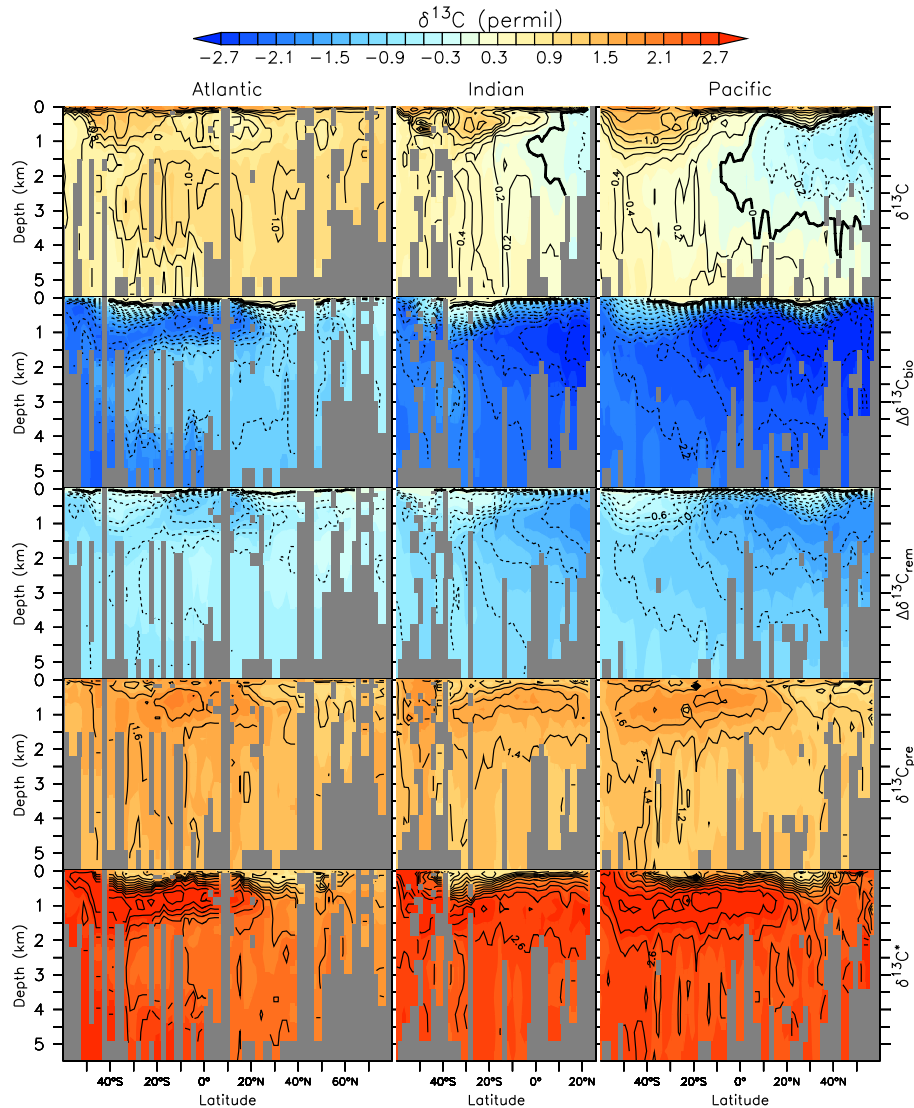


Fig. 11. As Fig. 6 but for the observations representing the 1990s.

patterns found in the observations, but they underestimate the AAIW maximum (Fig. 13). Preindustrial model results show much reduced vertical gradients of $\delta^{13}\text{C}^*$ in the thermocline (Fig. 6), indicating that the large gradients in the contemporary observations are partly caused by anthropogenic carbon.

The latitudinal distribution of the simulated anthropogenic $\delta^{13}\text{C}_{\text{DIC}}$ shift in the North Pacific is consistent with the data-based multi-parameter mixing model of Sonnerup et al. (2007), who found surface values ranging from 0.8 ‰ in the subtropics to 0.2–0.4 ‰ poleward of 40° N and vertical integrated values to be -200 ‰ m at high latitudes and -400 to -500 ‰ m at low latitudes. Along 165° E model FeL predicts for the 1990s -280 ‰ m around 45° N and -430 ‰ m at 30° N.

6 Summary, discussion, and conclusions

Comparison of a new three-dimensional model of ^{13}C cycling in the ocean with a new global database of $\delta^{13}\text{C}_{\text{DIC}}$ observations shows broad agreement in important large-scale features such as the vertical and inter-basin gradients. Our results support earlier findings, suggesting that effects of biological fractionation dominate the interior $\delta^{13}\text{C}_{\text{DIC}}$ distribution in the modern and pre-anthropogenic ocean, whereas the effect of air–sea gas exchange is to reduce the biologically imposed $\delta^{13}\text{C}_{\text{DIC}}$ gradients (MS00; Lynch-Stieglitz et al., 1995; Broecker and Maier-Reimer, 1992; Kroopnick, 1985). It is important to note that biologically created gradients are mediated by circulation and are therefore non-local. Considering the effects of gas exchange and biology on local $\delta^{13}\text{C}_{\text{DIC}}$ tendencies for surface waters, one may

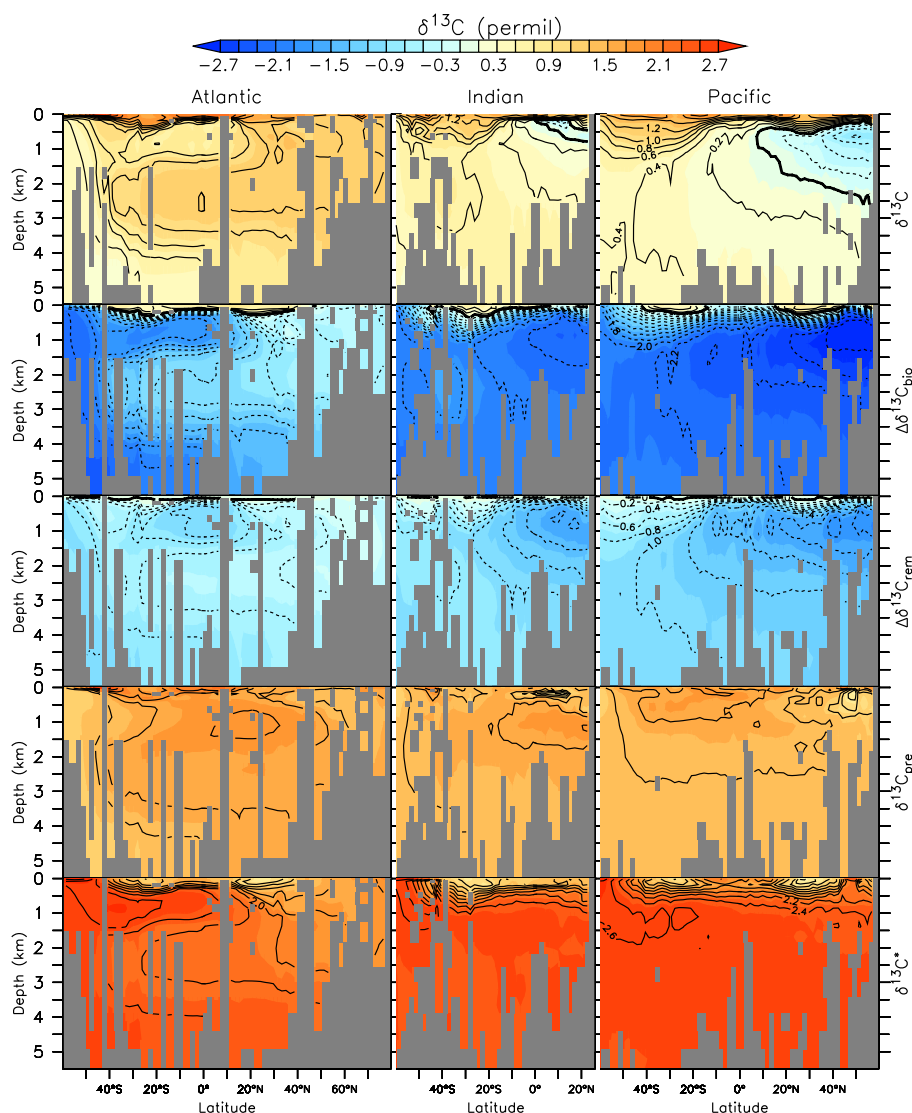


Fig. 12. As Fig. 6 but for the 1990s of model *FeL*.

conclude that they work together in some regions, such as the subpolar oceans where both tend to increase $\delta^{13}\text{C}_{\text{DIC}}$, but oppose each other in other regions, such as the subtropics where biology tends to increase $\delta^{13}\text{C}_{\text{DIC}}$ but gas exchange tends to decrease it (Fig. 3). However, whereas photosynthesis tends to increase $\delta^{13}\text{C}_{\text{DIC}}$ in high latitude surface waters, the overall effect of biology is to decrease $\delta^{13}\text{C}_{\text{DIC}}$ there due to upwelling of isotopically light, remineralized carbon from the deep ocean ($\Delta\delta^{13}\text{C}_{\text{bio}}$, Fig. 3). In contrast to previous studies that have attributed the effect of air–sea gas exchange only or mainly to the temperature-dependent fractionation (Charles et al., 1993; Broecker and Maier-Reimer, 1992; Lynch-Stieglitz et al., 1995; MS00), we have shown that temperature-independent air–sea fluxes acting only on biologically created gradients are equally important.

In contrast to previous conclusions (Gruber et al., 1999; Broecker and Maier-Reimer, 1992; Lynch-Stieglitz et al., 1995) that biological and air–sea gas exchange influences nearly cancel for surface $\delta^{13}\text{C}_{\text{DIC}}$ distributions, we find that the air–sea gas exchange, although acting to reduce the biological effect, is not able to cancel it for preindustrial times. This conclusion depends on the accuracy of the k_0 estimate (Eq. 3). Sensitivity tests with a slightly different model version than the one presented here show improvements of the $\delta^{13}\text{C}_{\text{DIC}}$ and $\Delta^{14}\text{C}_{\text{DIC}}$ simulations by using $k_0 = 0.253$ (NRMSEs of 0.53 and 0.26) compared with $k_0 = 0.337$ (NRMSEs of 0.56 and 0.29) supporting Sweeney et al. (2007) and Graven et al. (2012). Although we cannot exclude somewhat higher values of k_0 than used here, we believe that our results will be robust for modestly faster rates of air–sea gas exchange.

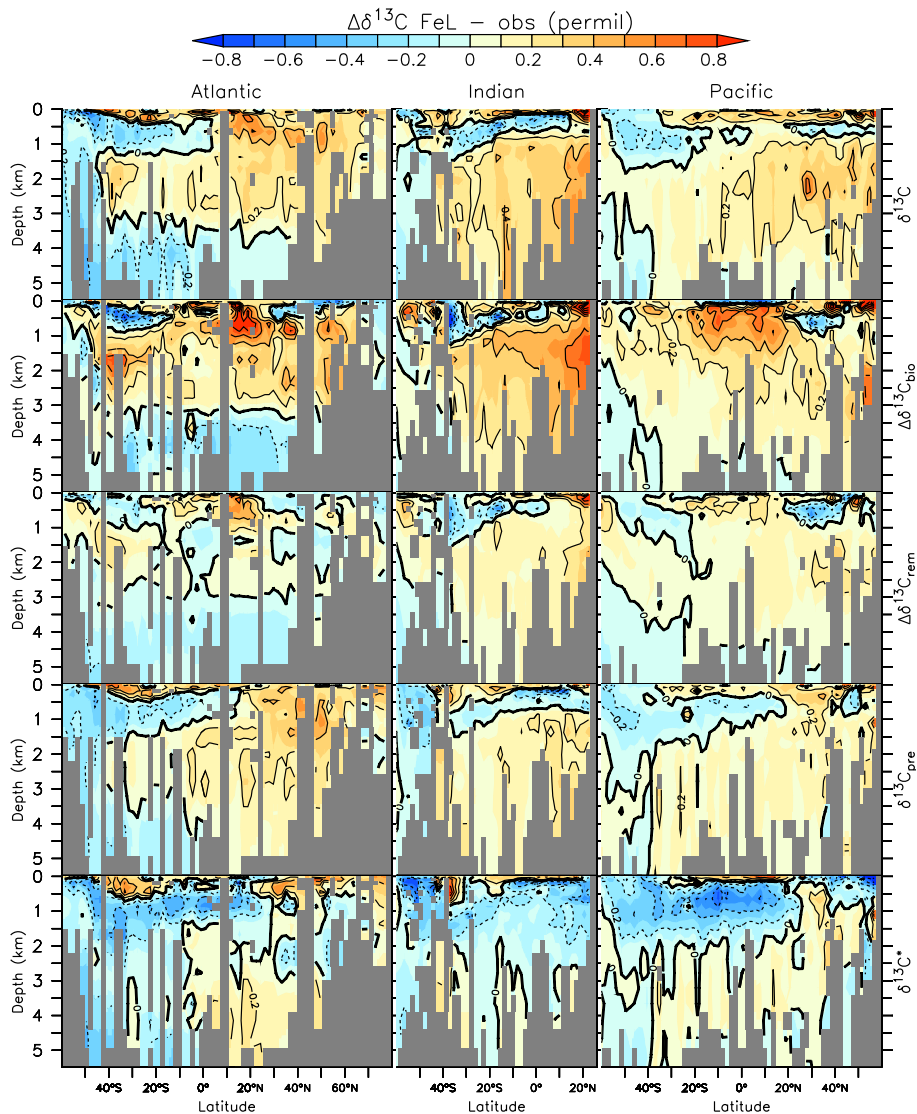


Fig. 13. As Fig. 6 but for difference model *FeL* minus observations.

Our model results suggest that the uptake of anthropogenic carbon has reduced the spatial gradients in $\delta^{13}\text{C}_{\text{DIC}}$ that were present in the preindustrial surface (and deep) ocean. The anthropogenic overprint is largest in the subtropics (Fig. 14), where it reduces the preindustrial $\delta^{13}\text{C}_{\text{DIC}}$ maximum (Figs. 3, 8). This may explain the different conclusions on the relative strength of biological vs. gas exchange effects on $\delta^{13}\text{C}_{\text{DIC}}$ reached previously based on analyzed observations affected by anthropogenic carbon (Gruber et al., 1999; Broecker and Maier-Reimer, 1992). Although the gas exchange effects are relatively minor in today's (modern and pre-anthropogenic) oceans, our model sensitivity tests suggest that changes in gas exchange rates could potentially be an important mechanism for changing the isotopic budget of the ocean interior in a different climate.

The effect of air–sea gas exchange on $\delta^{13}\text{C}_{\text{DIC}}$ depends on the residence time of waters at the surface, which depends on the circulation. Likewise, the effect of biology on deep ocean $\delta^{13}\text{C}_{\text{DIC}}$ depends on the circulation and mixing of different water masses. In this paper we did not directly address the sensitivity of $\delta^{13}\text{C}_{\text{DIC}}$ on circulation and mixing in the model. This will be left for future study. The fact that the model reproduces the observed distribution of $\delta^{13}\text{C}_{\text{DIC}}$ and the individual effects and components reasonably well suggests that it has the balance of circulation, gas-exchange, and biology about right, but it cannot be ruled out that compensating errors lead to the right result for the wrong reason or that other parameter combinations lead to a similarly good simulation. Thus, our results could be model dependent.

The model data comparison revealed a number of important model deficiencies, such as $\delta^{13}\text{C}_{\text{DIC}}$ values being

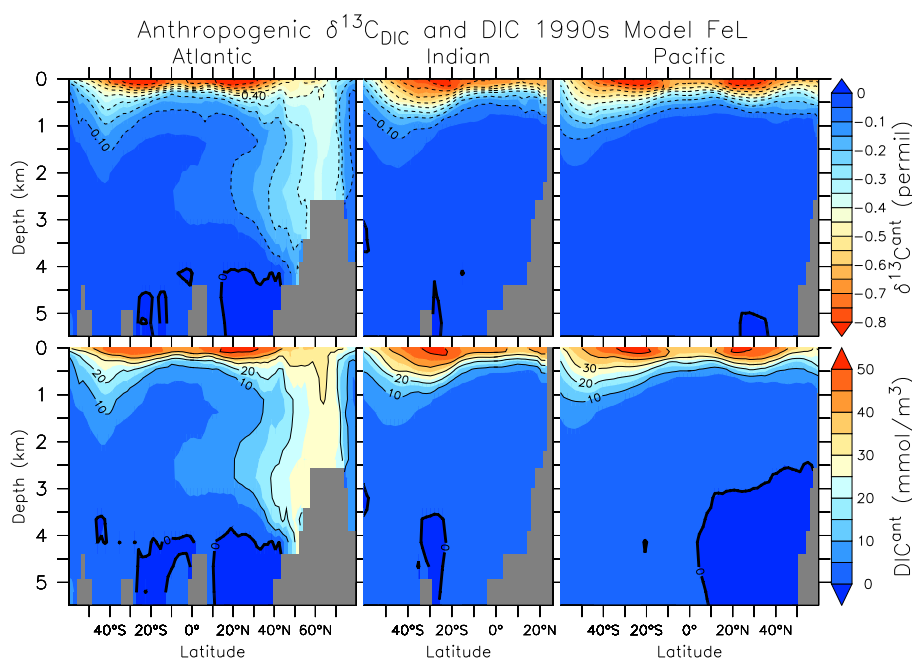


Fig. 14. Anthropogenic $\delta^{13}\text{C}$ (top) and carbon (bottom). Isoline difference is 0.1 ‰.

too high in the deep ocean, particularly the North Atlantic, Indian and North Pacific. Decomposition into the different components and effects may help in improving the model in the future, e.g. by improving AOU and/or preformed nutrient distributions. The model may be a useful tool for paleoclimate and other applications. The model (called Model of Ocean Biogeochemistry and Isotopes; MOBI version 0.2 = model *FeL*) code is freely available as a supplement to this paper and at <http://people.oregonstate.edu/~schmita2/data/schmittner13bg/>.

Appendix A

Observations

The primary data source for the $\delta^{13}\text{C}_{\text{DIC}}$ measurements is the Web Accessible Visualization and Extraction System (WAVES) at the Carbon Dioxide Information Analysis Center (CDIAC) (<http://cdiac3.ornl.gov/waves/discrete/>). On 27 August 2010 we extracted data from two databases within CDIAC: First, from the Global Data Analysis Project GLODAP (Key et al., 2004) and second, from the Carbon Dioxide in the Atlantic Ocean (CARINA) data synthesis project mainly from WOCE and CLIVAR expeditions (Key et al., 2010).

The $\delta^{13}\text{C}_{\text{DIC}}$ data on file at CDIAC have not been quality controlled. In the GLODAP database, some cruises (for example, 316N145_5 and INDIGO 123) had obvious bad data, and these were excluded from our compilation. From the remaining 31 GLODAP expeditions, we removed bottle num-

bers > 70 from seven cruises in order to exclude large volume (LV) samples, many of which had large negative biases. From the CARINA database, cruise 64TR19900417 was excluded due to obviously bad data, leaving 18 cruises. The remaining combined GLODAP and CARINA database contains 17 989 $\delta^{13}\text{C}_{\text{DIC}}$ data for the time period from 1990–2005 from all oceans and all depths. These data were supplemented by 632 measurements from 1990 to 1998 made at Charles (Dave) Keeling’s laboratory at Scripps Institution of Oceanography, described by Gruber et al. (1999), and by one transect (50 data points) from the northeast Pacific measured in Alan Mix’s laboratory at Oregon State University, published along with nutrient data by Ortiz et al. (2000). The Keeling dataset is also available at CDIAC (<http://cdiac.ornl.gov/ftp/oceans/keeling.data/>), although here we used one single data file provided by N. Gruber. We do not use measurements prior to 1990 (such as all GEOSECS and TTO data). Due to unresolved intercalibration issues between laboratories the accuracy is currently estimated to be 0.1–0.2 ‰ (A. McNichol, personal communication, 2012). The combined data set contains a total of 18 670 $\delta^{13}\text{C}_{\text{DIC}}$ measurements. It is freely available in the supplement to this paper, at CDIAC <http://cdiac3.ornl.gov>, at the National Oceanographic Data Center <http://www.nodc.noaa.gov/>, as well as here <http://people.oregonstate.edu/~schmita2/data/schmittner13bg>.

Supplementary material related to this article is available online at: <http://www.biogeosciences.net/10/5793/2013/bg-10-5793-2013-supplement.zip>.

Acknowledgements. We thank three anonymous referees for thoughtful and constructive comments that helped improve the paper. This work has been funded by the Paleoclimate and Marine Geology and Geophysics programs of the National Science Foundation through grants 0602395-ATM (Project PALEOVAR) and 1131834-OCE (Reconstructing Glacial Nitrogen and Carbon Cycling Using Isotopes) and N. G. acknowledges support by the EU grants 264879 (CARBOCHANGE) and 283080 (GEO-CARBON).

Edited by: F. Joos

References

- Anderson, L. A. and Sarmiento, J. L.: Redfield ratios of remineralization determined by nutrient data analysis, *Global Biogeochem. Cy.*, 8, 65–80, 1994.
- Allison, C. E., and Francey, R. J.: $\delta^{13}\text{C}$ of atmospheric CO_2 at Cape Grim: The in situ record, flask record, air standards and the CG92 calibration scale, in: *Baseline atmospheric Program (Australia)*, edited by: Gras, J. L., Derek, N., Tindale, N. W., and Dick, A. L., Bureau of Meteorology and CSIRO Atmospheric Research, 45–56, 1996.
- Berger, W. H. and Vincent, E.: Deep-sea carbonates – reading the carbon-isotope signal, *Geol. Rundsch.*, 75, 249–269, 1986.
- Boyd, P. W. and Ellwood, M. J.: The biogeochemical cycle of iron in the ocean, *Nat. Geosci.*, 3, 675–682, 2010.
- Broecker, W. S.: “NO” a conservative water-mass tracer, *Earth Planet. Sc. Lett.*, 23, 100–107, 1974.
- Broecker, W. S.: Ocean chemistry during glacial time, *Geochim. Cosmochim. Ac.*, 46, 1689–1705, 1982.
- Broecker, W. S. and Maier-Reimer, E.: The influence of air and sea exchange on the carbon isotope distribution in the sea, *Global Biogeochem. Cy.*, 6, 315–320, doi:10.1029/92gb01672, 1992.
- Broecker, W. S. and Peng, T. H.: *Tracers in the Sea*, Eldigio, Palisades, New York, 1982.
- Carpenter, E. J., Harvey, H. R., Fry, B., and Capone, D. G.: Biogeochemical tracers of the marine cyanobacterium *Trichodesmium*, *Deep-Sea Res. Pt. I*, 44, 27–38, 1997.
- Charles, C. D., Wright, J. D., and Fairbanks, R. G.: Thermodynamic influences on the marine carbon isotope record, *Paleoceanography*, 8, 691–697, doi:10.1029/93PA01803, 1993.
- Crowley, T. J.: Causes of climate change over the past 1000 years, *Science*, 289, 270–277, 2000.
- Curry, W. B. and Oppo, D. W.: Glacial water mass geometry and the distribution of $\delta^{13}\text{C}$ of ΣCO_2 in the western Atlantic Ocean, *Paleoceanography*, 20, PA1017, doi:10.1029/2004PA001021, 2005.
- Elrod, V. A., Berelson, W. M., Coale, K. H., and Johnson, K. S.: The flux of iron from continental shelf sediments: a missing source for global budgets, *Geophys. Res. Lett.*, 31, L12307, doi:10.1029/2004gl020216, 2004.
- Francey, R. J., Allison, C. E., Etheridge, D. M., Trudinger, C. M., Enting, I. G., Leuenberger, M., Langenfelds, R. L., Michel, E., and Steele, L. P.: A 1000-year high precision record of $\delta^{13}\text{C}$ in atmospheric CO_2 , *Tellus B*, 51, 170–193, 1999.
- Goericke, R. and Fry, B.: Variations of marine plankton $\Delta\text{C-13}$ with latitude, temperature, and dissolved CO_2 in the world ocean, *Global Biogeochem. Cy.*, 8, 85–90, 1994.
- Graven, H. D., Gruber, N., Key, R., Khatiwala, S., and Giraud, X.: Changing controls on oceanic radiocarbon: new insights on shallow-to-deep ocean exchange and anthropogenic CO_2 uptake, *J. Geophys. Res.*, 117, C10005, doi:10.1029/2012jc008074, 2012.
- Gruber, N. and Keeling, C. D.: An improved estimate of the isotopic air–sea disequilibrium of CO_2 : Implications for the oceanic uptake of anthropogenic CO_2 , *Geophys. Res. Lett.*, 28, 555–558, 2001.
- Gruber, N., Keeling, C. D., Bacastow, R. B., Guenther, P. R., Lueker, T. J., Wahlen, M., Meijer, H. A. J., Mook, W. G., and Stocker, T. F.: Spatiotemporal patterns of carbon-13 in the global surface oceans and the oceanic Suess effect, *Global Biogeochem. Cy.*, 13, 307–335, 1999.
- Hansen, B. W. and Jensen, F.: Specific growth rates of protozooplankton in the marginal ice zone of the central Barents Sea during spring, *J. Mar. Biol. Assoc. UK*, 80, 37–44, 2000.
- Hofmann, M., Wolf-Gladrow, D. A., Takahashi, T., Sutherland, S. C., Six, K. D., and Maier-Reimer, E.: Stable carbon isotope distribution of particulate organic matter in the ocean: a model study, *Mar. Chem.*, 72, 131–150, 2000.
- Houghton, R. A.: Balancing the Global Carbon Budget, *Annu. Rev. Earth Pl. Sc.*, 35, 313–347, doi:10.1146/annurev.earth.35.031306.140057, 2007.
- Ito, T. and Follows, M. J.: Preformed phosphate, soft tissue pump and atmospheric CO_2 , *J. Mar. Res.*, 63, 813–839, 2005.
- Keeling, C. D., Piper, S. C., Bacastow, R. B., Wahlen, M., Whorf, T. P., Heimann, M., and Meijer, H. A.: Exchanges of atmospheric CO_2 and $^{13}\text{CO}_2$ with the terrestrial biosphere and oceans from 1978 to 2000, I. Global aspects, *Scripps Institution of Oceanography*, 88 pp., 2001.
- Keller, K. and Morel, F. M. M.: A model of carbon isotopic fractionation and active carbon uptake in phytoplankton, *Mar. Ecol.-Prog. Ser.*, 182, 295–298, 1999.
- Keller, D. P., Oschlies, A., and Eby, M.: A new marine ecosystem model for the University of Victoria Earth System Climate Model, *Geosci. Model Dev.*, 5, 1195–1220, doi:10.5194/gmd-5-1195-2012, 2012.
- Key, R. M., Kozyr, A., Sabine, C. L., Lee, K., Wanninkhof, R., Bullister, J. L., Feely, R. A., Millero, F. J., Mordy, C., and Peng, T. H.: A global ocean carbon climatology: results from Global Data Analysis Project (GLODAP), *Global Biogeochem. Cy.*, 18, GB4031, doi:10.1029/2004GB002247, 2004.
- Key, R. M., Tanhua, T., Olsen, A., Hoppema, M., Jutterström, S., Schirnick, C., van Heuven, S., Kozyr, A., Lin, X., Velo, A., Wallace, D. W. R., and Mintrop, L.: The CARINA data synthesis project: introduction and overview, *Earth Syst. Sci. Data*, 2, 105–121, doi:10.5194/essd-2-105-2010, 2010.
- Kroopnick, P. M.: The distribution of C-13 of sigma- CO_2 in the world oceans, *Deep-Sea Res.*, 32, 57–84, 1985.
- Legrand, P. and Wunsch, C.: Constraints from paleotracer data on the North-Atlantic circulation during the last Glacial Maximum, *Paleoceanography*, 10, 1011–1045, 1995.
- Lynch-Stieglitz, J., Stocker, T. F., Broecker, W. S., and Fairbanks, R. G.: The influence of air-sea exchange on the isotopic composition of oceanic carbon – observations and modeling, *Global Biogeochem. Cy.*, 9, 653–665, 1995.
- Mahowald, N. M., Baker, A. R., Bergametti, G., Brooks, N., Duce, R. A., Jickells, T. D., Kubilay, N., Prospero, J. M., and Tegen, I.: Atmospheric global dust cycle and iron inputs to the ocean, *Global Biogeochem. Cy.*, 19, GB4025,

- doi:10.1029/2004gb002402, 2005.
- Marchal, O. and Curry, W. B.: On the abyssal circulation in the glacial Atlantic, *J. Phys. Oceanogr.*, 38, 2014–2037, 2008.
- Marchal, O., Stocker, T. F., and Joos, F.: A latitude-depth, circulation biogeochemical ocean model for paleoclimate studies, development and sensitivities, *Tellus B*, 50, 290–316, 1998.
- Menviel, L., Joos, F., and Ritz, S. P.: Simulating atmospheric CO_2 , ^{13}C and the marine carbon cycle during the Last Glacial–Interglacial cycle: possible role for a deepening of the mean remineralization depth and an increase in the oceanic nutrient inventory, *Quaternary Sci. Rev.*, 56, 46–68, doi:10.1016/j.quascirev.2012.09.012, 2012.
- Mix, A. C. and Fairbanks, R. G.: North Atlantic surface-ocean control of late Pleistocene deep-ocean circulation, *Earth and Planet. Sci. Lett.*, 73, 231–243, 1985.
- Murnane, R. J. and Sarmiento, J. L.: Roles of biology and gas exchange in determining the $\delta^{13}\text{C}$ distribution in the ocean and the preindustrial gradient in atmospheric $\delta^{13}\text{C}$, *Global Biogeochem. Cy.*, 14, 389–405, 2000.
- O’Leary, M. H.: Carbon isotopes in photosynthesis, *Bioscience*, 38, 328–336, 1988.
- Orr, J., Najjar, R., Sabine, C., and Joos, F.: Abiotic-HOWTO, 2000.
- Ortiz, J. D., Mix, A. C., Rugh, W., Watkins, J. M., and Collier, R. W.: Deep dwelling planktonic foraminifera of the northeastern Pacific Ocean reveal environmental control of oxygen and carbon isotopic disequilibria, *Geochim. Cosmochim. Ac.*, 60, 4509–4523, 1996.
- Ortiz, J. D., Mix, A. C., Wheeler, P. A., and Key, R. M.: Anthropogenic CO_2 invasion into the northeast Pacific based on concurrent $\delta^{13}\text{C}_{\text{DIC}}$ and nutrient profiles from the California Current, *Global Biogeochem. Cy.*, 14, 917–929, 2000.
- Popp, B. N., Takigiku, R., Hayes, J. M., Louda, J. W., and Baker, E. W.: The post-paleozoic chronology and mechanism of ^{13}C depletion in primary marine organic-matter, *Am. J. Sci.*, 289, 436–454, 1989.
- Quay, P., Sonnerup, R., Westby, T., Stutsman, J., and McNichol, A.: Changes in the $^{13}\text{C}/^{12}\text{C}$ of dissolved inorganic carbon in the ocean as a tracer of anthropogenic CO_2 uptake, *Global Biogeochem. Cy.*, 17, 1004, doi:10.1029/2001GB001817, 2003.
- Rau, G. H., Riebesell, U., and Wolf-Gladrow, D.: A model of photosynthetic ^{13}C fractionation by marine phytoplankton based on diffusive molecular CO_2 uptake, *Mar. Ecol.-Prog. Ser.*, 133, 275–285, 1996.
- Sarnthein, M., Stategger, K., Dreger, D., Erlenkeuser, H., Grootes, P., Haupt, B. J., Jung, S., Kiefer, T., Kuhnt, W., Pflaumann, U., Schäfer-Neth, C., Schulz, H., Schulz, M., Seidov, D., Simstich, J., van Kreveld, S., Vogelsang, E., A., V., and Weinelt, M.: Fundamental modes and abrupt changes in North Atlantic circulation and climate over the last 60 ky – concepts, reconstruction and numerical modeling, in: *The Northern North Atlantic: A Changing Environment*, edited by: Schäfer, P., Ritzau, W., Schlüter, M., and Thiede, J., Springer-Verlag, Berlin, 365–410, 2001.
- Schmitt, J., Schneider, R., Elsig, J., Leuenberger, D., Laurantou, A., Chappellaz, J., Köhler, P., Joos, F., Stocker, T. F., Leuenberger, M., and Fischer, H.: Carbon isotope constraints on the deglacial CO_2 rise from ice cores, *Science*, 336, 711–714, doi:10.1126/science.1217161, 2012.
- Schmittner, A. and Galbraith, E. D.: Glacial greenhouse-gas fluctuations controlled by ocean circulation changes, *Nature*, 456, 373–376, 2008.
- Schmittner, A., Oschlies, A., Matthews, H. D., and Galbraith, E. D.: Future changes in climate, ocean circulation, ecosystems, and biogeochemical cycling simulated for a business-as-usual CO_2 emission scenario until year 4000 AD, *Global Biogeochem. Cy.*, 22, GB1013, doi:10.1029/2007gb002953, 2008.
- Schmittner, A., Urban, N. M., Keller, K., and Matthews, H. D.: Using tracer observations to reduce the uncertainty of ocean diapy- mixing and climate-carbon cycle projections, *Global Biogeochem. Cy.*, 23, GB4009, doi:10.1029/2008GB003421, 2009a.
- Schmittner, A., Oschlies, A., Matthews, H. D., and Galbraith, E. D.: Correction to “Future changes in climate, ocean circulation, ecosystems, and biogeochemical cycling simulated for a business-as-usual CO_2 emission scenario until year 4000 AD”, *Global Biogeochem. Cy.*, 23, GB3005, doi:10.1029/2009gb003577, 2009b.
- Shackleton, N. J.: Carbon-13 in *Uvigerina*: tropical rainforest history and the Equatorial Pacific carbonate dissolution cycles, in: *The Fate of Fossil Fuel CO_2 in the Oceans*, edited by: Andersen, N. R. and Malahoff, A., 401–427, 1977.
- Shackleton, N. J.: The carbon isotope record of the Cenozoic history of organic carbon burial and of oxygen in the ocean and atmosphere, in: *Marine Petroleum Source Rocks*, edited by: Brooks, J. and Fleet, A. J., Geological Society Special Publication 236, 423–434, 1987.
- Shackleton, N. J., Le, J., Mix, A., and Hall, M. A.: Carbon isotope records from Pacific surface waters and atmospheric carbon-dioxide, *Quaternary Sci. Rev.*, 11, 387–400, 1992.
- Somes, C. J., Schmittner, A., and Altabet, M. A.: Nitrogen isotope simulations show the importance of atmospheric iron deposition for nitrogen fixation across the Pacific Ocean, *Geophys. Res. Lett.*, 37, L23605, doi:10.1029/2010gl044537, 2010.
- Sonnerup, R. E. and Quay, P. D.: ^{13}C constraints on ocean carbon cycle models, *Global Biogeochem. Cy.*, 26, GB2014, doi:10.1029/2010gb003980, 2012.
- Sonnerup, R. E., McNichol, A. P., Quay, P. D., Gammon, R. H., Bullister, J. L., Sabine, C. L., and Slater, R. D.: Anthropogenic $\delta^{13}\text{C}$ changes in the North Pacific Ocean reconstructed using a multiparameter mixing approach (MIX), *Tellus B*, 59, 303–317, 2007.
- Spero, H. J., Bijma, J., Lea, D. W., and Bemis, B. E.: Effect of seawater carbonate concentration on foraminiferal carbon and oxygen isotopes, *Nature*, 390, 497–500, 1997.
- Sweeney, C., Gloor, E., Jacobson, A. R., Key, R. M., McKinley, G., Sarmiento, J. L., and Wanninkhof, R.: Constraining global air–sea gas exchange for CO_2 with recent bomb ^{14}C measurements, *Global Biogeochem. Cy.*, 21, GB2015, doi:10.1029/2006GB002784, 2007.
- Tagliabue, A. and Bopp, L.: Towards understanding global variability in ocean Carbon-13, *Global Biogeochem. Cy.*, 22, GB1025, doi:10.1029/2007GB003037, 2008.
- Tschumi, T., Joos, F., Gehlen, M., and Heinze, C.: Deep ocean ventilation, carbon isotopes, marine sedimentation and the deglacial CO_2 rise, *Clim. Past*, 7, 771–800, doi:10.5194/cp-7-771-2011, 2011.
- Turner, J. V.: Kinetic fractionation of ^{13}C during calcium-carbonate precipitation, *Geochim. Cosmochim. Ac.*, 46, 1183–1191, 1982.

- Weaver, A. J., Eby, M., Wiebe, E. C., Bitz, C. M., Duffy, P. B., Ewen, T. L., Fanning, A. F., Holland, M. M., MacFadyen, A., Matthews, H. D., Meissner, K. J., Saenko, O., Schmittner, A., Wang, H. X., and Yoshimori, M.: The UVic Earth System Climate Model: model description, climatology, and applications to past, present and future climates, *Atmos. Ocean*, 39, 361–428, 2001.
- Westberry, T., Behrenfeld, M. J., Siegel, D. A., and Boss, E.: Carbon-based primary productivity modeling with vertically resolved photoacclimation, *Global Biogeochem. Cy.*, 22, GB2024, doi:10.1029/2007GB003078, 2008.
- White, J. W. C. and Vaughn, B. C.: Stable isotopic composition of atmospheric carbon dioxide (^{13}C and ^{18}O) from the NOAA ESRL Carbon Cycle Cooperative Global Air Sampling Network, 1900–2010, <ftp://ftp.cmdl.noaa.gov/ccg/co2c13/flask/event/>, (last access 21 September 2012), 2011.
- Zhang, J., Quay, P. D., and Wilbur, D. O.: Carbon-isotope fractionation during gas-water exchange and dissolution of CO_2 , *Geochim. Cosmochim. Ac.*, 59, 107–114, 1995.